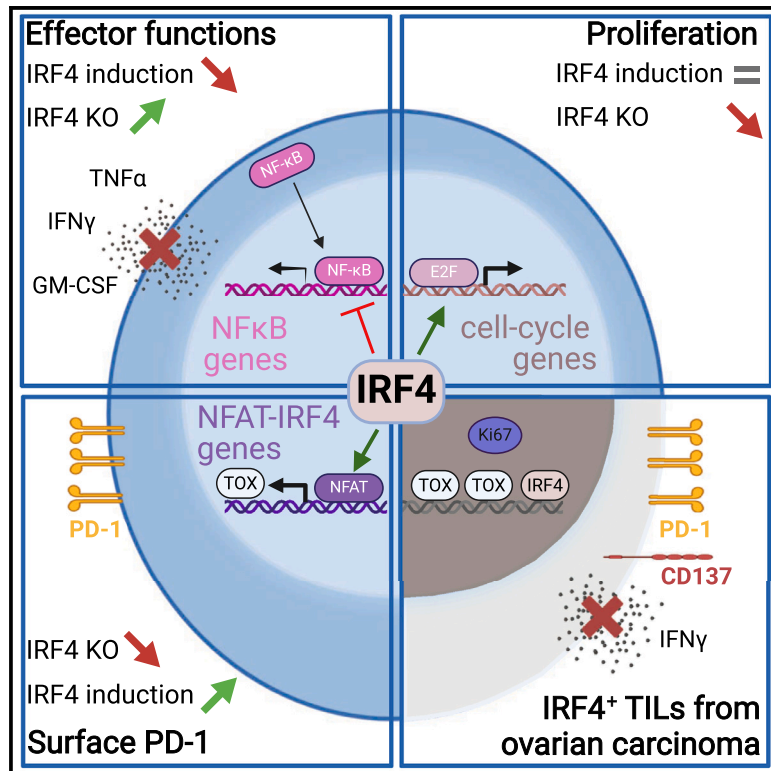# IRF4 impedes human CD8 T cell function and promotes cell proliferation and PD-1 expression

Graphical abstract

Authors

Thibault Hirsch, Damien Neyens, Céline Duhamel, ..., Virginie Montiel, Mélanie Deschamps, Pierre van der Bruggen

Correspondence

thibault.hirsch@uclouvain.be

In brief

Hirsch et al. subjected primary human CD8 T cells to IRF4 overexpression or knockout and assessed T cell functions and the transcriptome. The TCR-induced transcription factor IRF4 promotes proliferation and PD-1 expression but hampers effector functions and expression of NF-κB-regulated genes. They also compared CD8 tumor-infiltrating lymphocytes to activated T cells in patients with COVID-19.

Highlights

- IRF4 impairs cytokine production in human CD8 T cells

- IRF4 promotes PD-1 expression and T cell proliferation

- IRF4 regulates cell cycle genes and impairs NF-κB-regulated gene expression

- Exhaustion features in TILs are correlated to their activation and IRF4 expression

Article

IRF4 impedes human CD8 T cell function and promotes cell proliferation and PD-1 expression

Thibault Hirsch,[1,6,*] Damien Neyens,[1] Céline Duhamel,[1] Alexandre Bayard,[1] Christophe Vanhaver,[1] Mathieu Luyckx,[1,2] Francisco Sala de Oyanguren,[3] Claude Wildmann,[1] Nicolas Dauguet,[1] Jean-Luc Squifflet,[2] Virginie Montiel,[4] Mélanie Deschamps,[4] and Pierre van der Bruggen[1,5]

[1]De Duve Institute, Université Catholique de Louvain, Brussels, Belgium
[2]Département de Gynécologie, Cliniques Universitaires Saint-Luc, Brussels, Belgium
[3]Flow Cytometry Facility, University of Lausanne, Lausanne, Switzerland
[4]Unité de Soins Intensifs, Cliniques Universitaires Saint-Luc, Brussels, Belgium
[5]WELBIO Department, WEL Research Institute, Wavre, Belgium
[6]Lead contact
*Correspondence: thibault.hirsch@uclouvain.be
https://doi.org/10.1016/j.celrep.2024.114401

SUMMARY

Human CD8 tumor-infiltrating lymphocytes (TILs) with impaired effector functions and PD-1 expression are categorized as exhausted. However, the exhaustion-like features reported in TILs might stem from their activation rather than the consequence of T cell exhaustion itself. Using CRISPR-Cas9 and lentiviral overexpression in CD8 T cells from non-cancerous donors, we show that the T cell receptor (TCR)-induced transcription factor interferon regulatory factor 4 (IRF4) promotes cell proliferation and PD-1 expression and hampers effector functions and expression of nuclear factor κB (NF-κB)-regulated genes. While CD8 TILs with impaired interferon γ (IFNγ) production exhibit activation markers IRF4 and CD137 and exhaustion markers thymocyte selection associated high mobility group box (TOX) and PD-1, activated T cells in patients with COVID-19 do not demonstrate elevated levels of TOX and PD-1. These results confirm that IRF4⁺ TILs are exhausted rather than solely activated. Our study indicates, however, that PD-1 expression, low IFNγ production, and active cycling in TILs are all influenced by IRF4 upregulation after T cell activation.

INTRODUCTION

In mouse models of chronic lymphocytic choriomeningitis virus (LCMV) infection and cancer, antigen persistence causes memory precursor CD8 T cells to differentiate into exhausted CD8 T cells.[1–7] These cells have a specific transcriptomic and epigenetic program that confers them a stable identity; altered effector functions, such as diminished cytokine production; and expression of inhibitory receptors, such as PD-1.[8] In patients with cancer, high PD-1 expression identifies the tumor-infiltrating lymphocytes (TILs) with the weakest ability to produce cytokines.[9–11] Furthermore, the transcription factor TOX, which is critical for exhausted T cell development, is coexpressed in CD8 T cells with high PD-1 expression in patients with cancer and those chronically infected with the hepatitis C virus.[12–14] However, TOX is also expressed in functionally competent effector memory CD8 T cells from the blood of healthy donors, thus suggesting that the sole detection of TOX is not a proof of exhaustion.[15] Moreover, single-cell RNA sequencing (RNA-seq) analysis of human TILs revealed that cells expressing genes encoding exhaustion markers, like PD-1 or TIM-3, are clonally expanded and cycling and express genes encoding activation markers like CD137.[11,16–21] These observations raise the question of whether TILs are exhausted or simply activated and illus-

trate the difficulty of distinguishing activated from exhausted T cells. This is because important overlap exists between T cell activation and exhaustion, as the latter originates in T cell receptor (TCR) signaling.[13,14,22] Thus, assessment of T cell functions is classically performed to discriminate activated from exhausted CD8 T cells.

In both the mouse model of LCMV chronic infection and patients with cancer, PD-1⁺ CD8 T cells expressing several inhibitory receptors are more dysfunctional than simple PD-1⁺-expressing cells.[10,23–25] As expression of multiple inhibitory receptors is tightly associated with T cell activation,[11,16–21] this again raises the question of whether the observed defect is not simply due to recent T cell activation. Interestingly, when exhausted CD8 T cells are left to rest several weeks, they partially recover their effector functions and have lower inhibitory receptor expression, and their transcriptomic profile diverges from the exhaustion signature.[26] Thus, exhaustion-like features reported in human TILs could partly be the reflection of their activation rather than the consequence of bona fide T cell exhaustion.

The transcription factor IRF4 is well known to be quickly upregulated after TCR activation, and the magnitude of IRF4 expression is proportional to the strength of TCR activation.[27,28] However, contradictory reports have been published as to the role of IRF4 in mouse T cells. During acute viral infection, IRF4 is
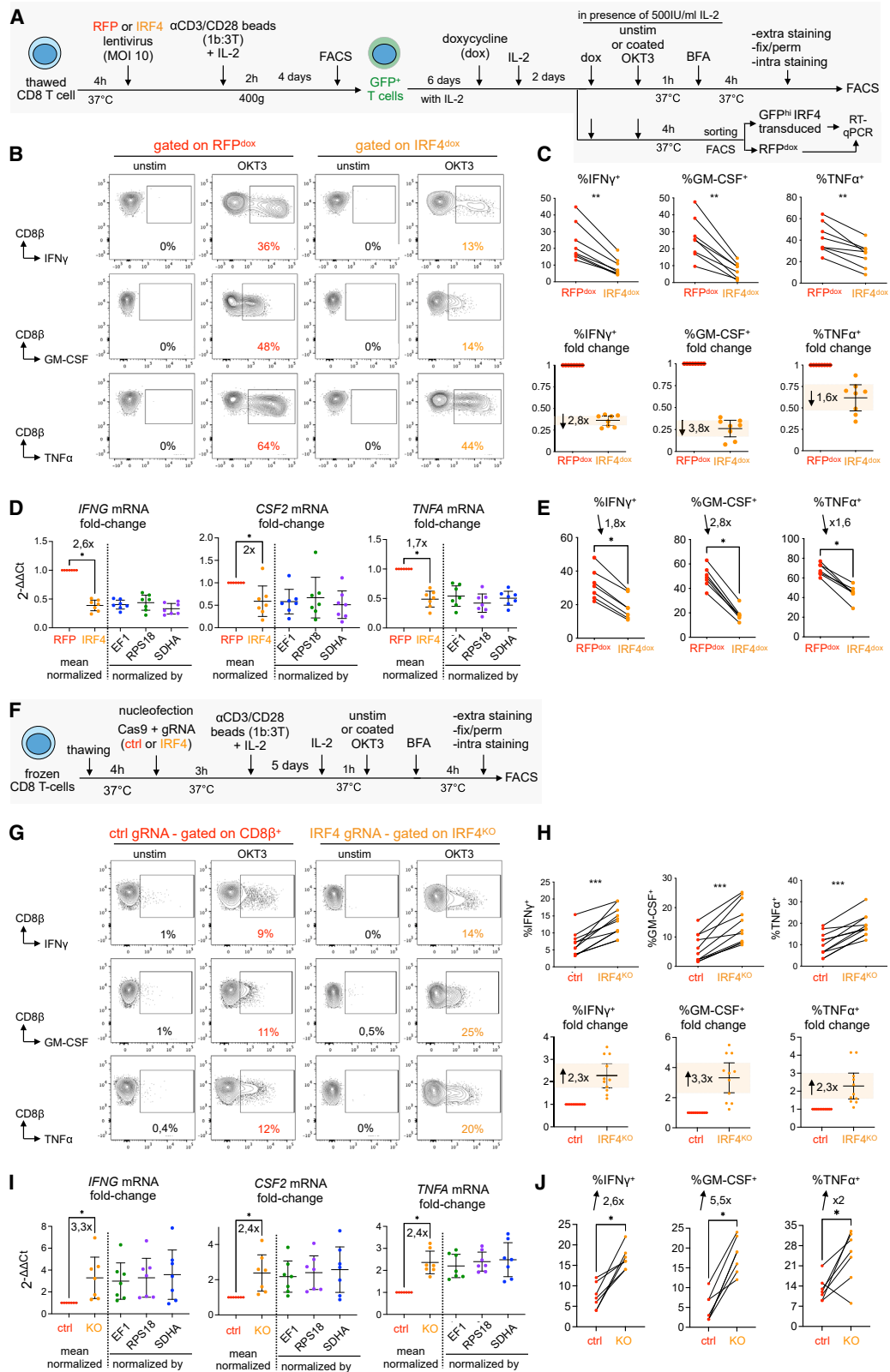
required for CD8 T cell function, as its expression sustains naive T cell differentiation into effector cells, as well as their expansion and glycolysis.[27,28] Similarly, in a model of transplant rejection by CD4 T cells, IRF4 is required for allograft rejection by sustaining T cell function and restraining PD-1 expression.[29] Conversely, during chronic viral infection, IRF4 impairs exhausted CD8 T cell function and glycolysis and is required for PD-1 expression.[30] In addition to these contradictory reports, no data have been published as to the role of IRF4 in human CD8 T cells, both in normal and pathological conditions.

In this work, we subjected CD8 T cells from non-cancerous donors to IRF4 overexpression or knockout (KO) and assessed the impact of these modifications on T cell functions and transcriptome. We then correlated our findings with analysis of human TILs from ovarian carcinoma samples for IRF4 and exhaustion markers expression. We finally determined whether expression of these exhaustion markers is not solely due to TIL activation by comparing them to activated T cells in the blood of patients with COVID-19.

RESULTS

IRF4 impairs cytokine production in human CD8 T cells

To identify any regulatory function of IRF4 in activated CD8 T cells, we first aimed to force IRF4 expression once the activation peak of CD8 T-cells was passed and to assess T cell function upon reactivation. We first tracked the expression dynamics of proteins commonly expressed by activated and exhausted T cells, such as PD-1, LAG-3, IRF4, and basic leucine zipper ATF-like transcription factor (BATF), which showed synchronized expression with the activation marker CD137 (Figures S1A and S1B). These proteins returned to basal levels around days 10–12, indicating that the T cell activation peak was passed. We transduced and amplified CD8 T cells with lentiviruses bearing a doxycycline-responsive promoter so as to control the timing of induction of IRF4 or its control gene encoding the red fluorescent protein (RFP) and triggered gene overexpression at day 10 post stimulation for 48 h with doxycycline (Figures S1C–S1E). Gene overexpression occurred only in around 45% of GFP-infected cells, so we specifically gated on RFP^{dox} or IRF4^{dox} cells for analysis requiring cell fixation and permeabilization, with the latter degrading GFP (Figures S1D–S1F).

For sorting of live cells by fluorescence-activated cell sorting (FACS), we used high GFP expression as a proxy to enrich for IRF4-overexpressing cells since gene overexpression triggered by doxycycline occurs in GFP^{hi} cells (Figure S1G).

CD8 T cells cultured for 48 h with doxycycline were reactivated with anti-CD3 (Figure 1A). Compared with their RFP^{dox} counterparts, fewer IRF4^{dox} cells produced cytokines (Figures 1B and 1C). Furthermore, FACS-sorted IRF4-infected GFP^{hi} cells (Figure S1G) had downregulation of cytokine-encoding mRNA, which resulted in diminished cytokine production (Figures 1D and 1E). Thus, ectopic expression of IRF4 in CD8 T cells impairs cytokine production, suggesting that TCR-induced expression of IRF4 might also impair cytokine production.

We performed CRISPR-Cas9 before T cell stimulation to prevent IRF4 upregulation and expanded the cells for 5 days, when activation markers were highly expressed (Figures 1F and S1B). IRF4^{KO} CD8 T cells exhibited increased cytokine production (Figures 1G, 1H, S1H, and S1I). We then used an optimized CRISPR-Cas9 protocol to reach 90% KO (Figures S1J–S1L), allowing us to FACS-sort live T cells for RNA extraction and RT-qPCR. Upon anti-CD3 reactivation, IRF4^{KO} cells had increased cytokine production and upregulated the corresponding mRNA (Figures 1I and 1J). Thus, IRF4 acts as a regulator of cytokine production in recently activated T cells.

To confirm these findings in the tumoral context, we transduced two human tumoral cell lines with a lentiviral construct encoding a single-chain variable fraction (scFv) of the OKT3 anti-CD3 antibody (Figures 2A and 2B).[31] Coculture of human CD8 T cells with the tumor cell lines showed that IRF4^{KO} T cells produced more cytokines and have improved degranulation ability, suggesting that IRF4 may also impair T cell cytotoxicity (Figures 2C–2F). Of note, no allogeneic reaction toward tumor cells was observed within the 5-h incubation time, thus testifying that the observed differences only came from CD3 cross-linking by the anti-CD3 scFv displayed on the tumor cell surface. Altogether, our data demonstrate that the presence of IRF4 restricts the effector functions of recently activated CD8 T cells.

IRF4 promotes human CD8 T cell proliferation and expansion

During culture of IRF4^{KO} CD8 T-cells, these cells seemed to proliferate slower than their control counterparts. Fluorescent cell

---

Figure 1. IRF4 impairs cytokine production in CD8 T cells isolated from non-cancerous donors

(A) Experiment overview. 1b:3T, 1 bead for 3 T cells.

(B) Representative examples of cytokine production.

(C) Percentage of cells producing the indicated cytokine. The fold change of IRF4^{dox} cells producing cytokines is shown with the error bars depicting mean value and 95% confidence interval (orange area) (8 donors, 3 independent experiments).

(D) mRNA levels assessed by RT-qPCR after FACS sorting of RFP or GFP^{hi} (IRF4) cells. The fold change was calculated with each reference gene. Error bars indicate mean + 95% confidence interval (7 donors, 2 independent experiments).

(E) Cytokine production in samples used for RT-qPCR.

(F) Experiment overview. 1b:3T, 1 bead for 3 T cells.

(G) Representative examples of cytokine production.

(H) Percentage of cells producing the indicated cytokine. The fold change of IRF4^{KO} cells producing cytokines is shown with the error bars depicting mean value and 95% confidence interval (orange area) (11 donors, 3 independent experiments).

(I) mRNA levels assessed by RT-qPCR after FACS sorting of control (ctrl) or KO CD8 T cells. The fold change was calculated with each reference gene. Error bars indicate mean + 95% confidence interval (7 donors, 2 independent experiments).

(J) Cytokine production in samples used for RT-qPCR.

$*p < 0.05$, $**p < 0.01$, $***p < 0.001$ (Wilcoxon matched pairs). See also Figure S1.

A Lentiviral construct to express anti-CD3 scFv on the tumor cell surface.
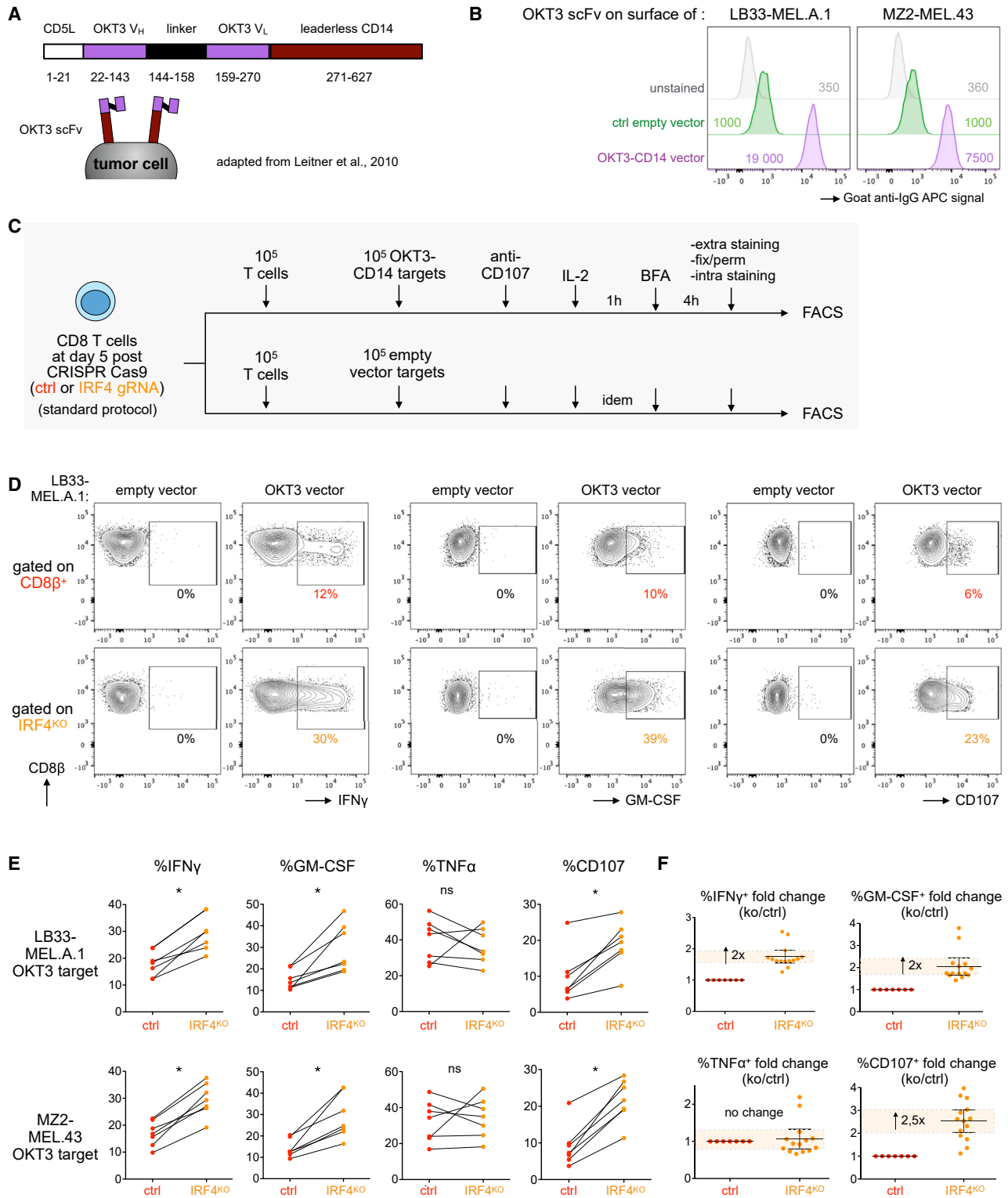
Figure 2. IRF4 impairs cytokine production and degranulation in human CD8 T cells activated by tumor cells

(A) Lentiviral construct to express anti-CD3 scFv on the tumor cell surface.

(B) The human tumoral cell lines LB33-MEL.A.1 and MZ2-MEL.43 transduced with the OKT3 scFv construct (purple) or control vector (green) were cloned. Surface expression of OKT3 scFv was measured with an allophycocyanine (APC)-coupled goat anti-immunoglobulin G antibody.

tracker dilution confirmed this observation, as 4 days after activation with anti-CD3/CD28 beads, the expansion and number of divisions of IRF4[KO] cells were 2.4 times lower (Figures 3A–3C). The proliferation pace of the IRF4[KO] cells that divided was close to their normal counterparts, suggesting that once a cell committed to proliferation, the absence of IRF4 had mild effects. Rather, IRF4 seemed to be involved in initiating cell proliferation, as the fraction of cells that initially divided was 2 times lower in IRF4[KO] cells (Figure 3C). Similar results were obtained when cells were activated with anti-CD3 alone or in combination with anti-CD28 (Figures S2A–S2I). Lower proliferation metrics calculated with cell tracker dilution ultimately resulted in lower IRF4[KO] cell yield (Figure S2J). Altogether, the promotion of cell proliferation and expansion by IRF4 is associated with molecular events downstream of TCR signaling rather than CD28 signaling.

We also investigated whether IRF4 overexpression enhances proliferation of CD8 T cells. We thawed and re-activated lentivirally transduced CD8 T cells. Despite its abundance in IRF4[dox] cells, IRF4 did not increase their proliferation (Figures S2K–S2M). These data suggest that the levels of endogenously synthetized IRF4 upon TCR activation were not limiting for T cell proliferation.

IRF4 is required for sustained PD-1 and TOX expression

IRF4 plays a dual role in activated CD8 T cells by inhibiting their effector functions while promoting their proliferation. Regulation of the function of proliferating T cells is reminiscent of the action of PD-1, for whom the effect of IRF4 on PD-1 expression is unclear in mice.[29,30] Since IRF4 facilitates the TCR-induced proliferation of CD8 T cells, any modification of PD-1 expression that might be observed could be attributed to an activation defect of CD8 T cells rather than a direct role of IRF4 in regulation of PD-1 expression. We thus tracked the expression of activation markers along the stage of cell division by labeling cells with a fluorescent cell tracker and monitoring Ki67 to distinguish between quiescent and cycling cells.

In response to anti-CD3/CD28 bead activation, both control and IRF4[KO] cells that had not entered the cell cycle (Ki67⁻ G0 cells) upregulated the activation markers CD137 and CD69 and the transcription factor BATF (Figures 3D and 3E). Upon entry into the cell cycle, BATF and CD137 were further upregulated in both conditions (Figures 3D and 3E). Interestingly, undivided IRF4[KO] cells showed stronger CD69 upregulation, and the return to baseline expression was delayed in dividing IRF4[KO] cells (Figure 3E). A similar trend was observed with CD137. Thus, IRF4[KO] cells showed signs of activation, whether they are proliferating or not. However, while PD-1 upregulation was observed in undivided IRF4[KO] cells, their ability to further increase PD-1 expression after cell division was impaired (Figures 3D and 3E).

Furthermore, fewer IRF4[KO] cells upregulated TOX after activation (Figures 3F–3H).

Using our optimized CRISPR-Cas9 protocol, we sorted alive CD8 T cells 45 h after activation (Figures S3A and S3B). We found lower PD-1 protein and mRNA in IRF4[KO] cells (Figures S3C and S3D). Altogether, our findings demonstrate that IRF4 is required for PD-1 and TOX expression in activated and proliferating human CD8 T cells.

Abundance of IRF4 exacerbates PD-1 expression and requires nuclear factor of activated T-cells (NFAT) activity

We observed that CD8 T cell activation with coated anti-CD3 supplemented or not with anti-CD28 triggered less PD-1 expression than anti-CD3/CD28 bead activation. Consequently, the difference in PD-1 expression between normal and IRF4[KO] cells was less prominent compared with anti-CD3/CD28 bead-activated T cells (Figures S3E–S3I). At the same time, IRF4 expression was lower in response to coated anti-CD3 as compared with bead activation (Figures S3J and S3K). We thus wondered whether amounts of IRF4 synthetized upon TCR activation modulate PD-1 abundance.

We thawed and re-activated lentivirus-transduced CD8 T cells, which had baseline levels of PD-1 expressed before reactivation (Figures 4A and 4B). After 72-h reactivation, IRF4[dox] T cells exhibited significantly higher PD-1 levels, while TOX, which also increases PD-1 when overexpressed, remained unchanged (Figures 4C–4E). Thus, the IRF4-mediated increase of PD-1 was not due to TOX upregulation. We then analyzed the role of NFAT, a well-described transcriptional partner of IRF4, in the regulation of PD-1 by IRF4. T cells activated in the presence of the NFAT inhibitor FK506 had lower PD-1 expression (Figures 4G and 4H). However, IRF4 upregulation was also impaired by FK506. By contrast, addition of the nuclear factor κB (NF-κB) inhibitor IKK16 had much less impact on PD-1 and IRF4 upregulation (Figures 4G and 4H), despite showing inhibition of NF-κB signaling, as indicated by CD69 downregulation. Consequently, impaired PD-1 expression could also result from blunted IRF4 upregulation rather than solely NFAT inhibition. We thus used IRF4-overexpressing T cells that maintain high IRF4 levels in the presence of an NFAT inhibitor (Figures 4I and 4J). Upon activation in presence of FK506, these cells lost PD-1 expression, while IKK16 had less and variable effect (Figures 4I–4K). Thus, our data indicate that IRF4 requires NFAT activity for PD-1 expression.

While there was a strong correlation between heightened PD-1 on the surface of IRF4[dox] cells and increased PDCD1 expression, IRF4[dox] cells with more PD-1 protein did not necessarily have higher PDCD1 mRNA (Figures S3L–S3N). Furthermore, we observed that, for two samples, there was lower PDCD1 mRNA and PD-1 protein at 45 h after activation (Figures S3N

(C) Experiment overview.

(D) Representative examples of cytokine production and degranulation (CD107).

(E) Percentage of cells producing the indicated cytokine or performing degranulation upon activation by OKT3-expressing targets (7 donors, 2 independent experiments). *$p < 0.05$ (Wilcoxon matched pairs).

(F) The fold change of the IRF4[KO] cells producing cytokines or performing degranulation with the error bars depicting mean value and 95% confidence interval (orange area). Graphs were made based on data from (E), pooling data obtained with the 2 targets.
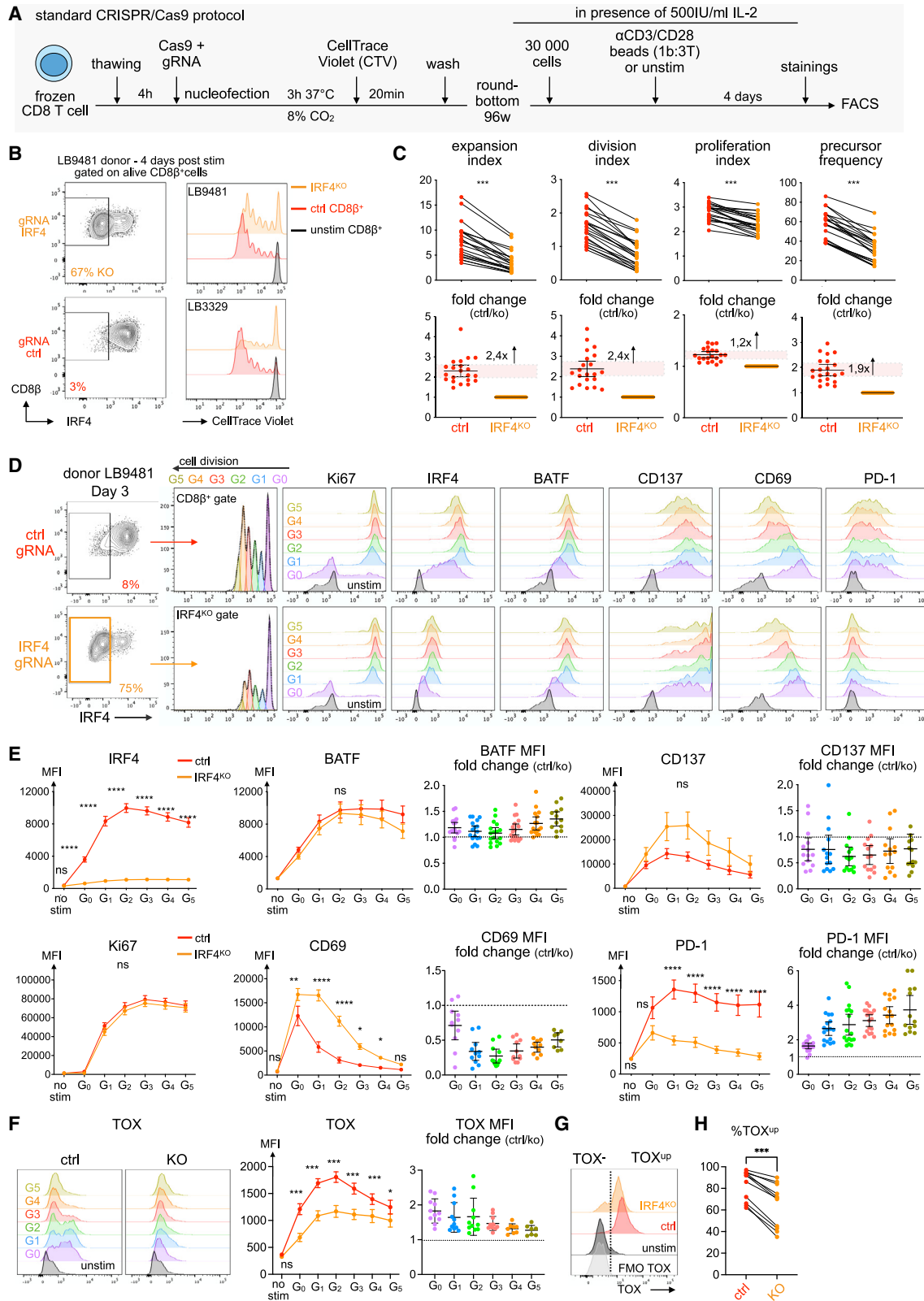
(legend on next page)

and S3O). However, at 72 h of activation, IRF4[dox] cells in these two samples displayed higher PD-1 levels than control RFP[dox] cells (Figure S3P). Thus, heightened levels of PD-1 proteins mediated by IRF4 are not solely the consequence of increased *PDCD1* gene transcription.

IRF4 regulates cell cycle gene expression and impairs NF-κB-regulated gene expression

To explore the molecular pathways involved in IRF4-dependent regulation of T cells proliferation and function, we used a method for analysing RNA following intracellular sorting to analyze the transcriptome of fixed and permeabilized CD8 T cells.[32] Day-5 IRF4[KO] and day-12 IRF4 overexpressing (IRF4[dox]) CD8 T cells were reactivated or not, FACS sorted, and subjected to RNA-seq (Figures S4A–S4D).

Transcriptional changes were observed in IRF4[KO] cells, regardless of T cell reactivation (Figures 5A, 5B, S4E, and S4F). This was partially reflected by altered proliferation of cultured IRF4[KO] cells before sorting, as evidenced by negative enrichment score of cell cycle genes analyzed by gene set enrichment analysis (GSEA). Conversely, IRF4 overexpression was sufficient to increase expression of these genes without reactivation of IRF4[dox] T cells (Figure 5C; Tables S1 and S2). This cell cycle gene set is regulated by E2F transcription factors, whose activity peaks at G1/S phase transition and is regulated by cyclin-CDK (cyclin-dependent kinase) complexes.[33] In line with this observation , IRF4 upregulated *CDK2*, which promotes G1/S phase transition by associating with cyclin E (Figure 5D). Furthermore, IRF4 downregulated *CDKN1A*, which inhibits CDK2-cyclin E activity, and IRF4[KO] cells also had increased *CDKN2A*, which inhibits CDK4/6-cyclin D activity (Figure 5E). The methyltransferase *EZH2*, a repressor of *CDKN2A*,[34] was also upregulated by IRF4 (Figure 5F). These findings indicate that IRF4 balances gene expression in favor of cell cycle progression, consistent with its role in CD8 T cell proliferation.

Upon reactivation, IRF4[KO] T cells exhibited enriched expression of NF-κB-regulated genes, while the opposite was observed in IRF4[dox] T cells (Figure 5G; Tables S1 and S2). Similar data were observed in non-reactivated T cells, but with a lower enrichment score (Table S2). We confirmed this GSEA with another set of NF-κB target genes (Figure 5H; Tables S1 and S2). The enrichment score obtained with the two NF-κB signatures tested was not solely due to genes that are common to both signatures (Figure S4G). These findings indicate that IRF4 inhibits expression of NF-κB-regulated genes, consistent with our results demonstrating that IRF4 impairs cytokine production

(Figure 1). Interestingly, IRF4 led to decreased expression of the NF-κB transcription factor c-Rel (Figure 5I). Furthermore, in non-reactivated cells, IRF4 upregulated Trib1 (Figure 5J), which has been shown to impair the formation of the CARMA1-Bcl10-MALT1 complex essential for NF-κB signal propagation.[35] Thus, IRF4 might impair NF-κB signaling upon TCR activation.

We assessed whether IRF4 overexpression impairs the canonical NF-κB signaling pathway by analyzing the nuclear translocation of the NF-κB subunit RelA (Figures S5A and S5B). We monitored the translocation after 30-min to 3-h TCR activation. As a control of impaired RelA translocation, we used the NF-κB signaling inhibitor IKK16, which indeed decreased RelA translocation and cytokine production in control RFP[dox] CD8 T cells (Figures S5C–S5F). When IRF4[dox] cells were compared to RFP[dox] cells, no difference in RelA translocation was detected despite diminished cytokine production in IRF4[dox] cells, as shown previously (Figures S5E–S5G). Our observations thus indicate that decreased expression of NF-κB-regulated genes by IRF4 does not come from altered NF-κB signaling to RelA.

IRF4 is expressed in human CD8 TILs with exhaustion and activation markers

Our transcriptomic analysis also revealed that IRF4 did not promote enrichment of a core exhaustion-specific gene signature validated in individuals with lung cancer and HIV[36] (Figures 5K and 5L; Tables S1 and S2). An exception stood out in IRF4[dox] cells, where genes downregulated in exhausted T cells were also found to be downregulated in IRF4[dox] cells (Figure 5L; Tables S1 and S2). Furthermore, IRF4 promoted the enrichment of a cluster of genes associated with the cell cycle, cell division, and cell proliferation, which are upregulated in non-small cell lung cancer (NSCLC) PD-1^{hi} TILs[11] (Figure 5M; Tables S1 and S2). Thus, we thoroughly analyzed by FACS the presence of IRF4 in TILs from ovarian carcinoma samples using activation, cycling, and exhaustion markers (Figures S6A and S6B).

We found distinct T cell subsets based on PD-1 or TOX expression levels, proteins used to identify exhausted T cells (Figures 6A and 6B). As reported, PD-1^{hi} and TOX^{hi} cells were the same cells (Figures 6C, S6C, and S6D).[13,14] We also detected TOX and PD-1 in the blood of non-cancerous donors,[15] but the PD-1^{hi} TOX[hi] population was found exclusively in tumor samples, where it accounted for 50% of CD8 TILs (Figures S6C and S6D). These findings highlight that TOX expression levels reported in blood CD8 T cells from healthy donors differs from levels detected in TILs.[15] Thus, by using this PD-1 stratification strategy,

---

Figure 3. IRF4 promotes human CD8 T cell proliferation and PD-1 expression

(A) Experiment overview. 1b:3T, 1 bead for 3 T cells.

(B) Examples of cell tracker dilution.

(C) Different proliferation metrics were calculated for each donor. The fold change is shown with the error bars depicting mean value and 95% confidence interval (red area). ***$p < 0.001$ (Wilcoxon matched pairs). 21 donors, 6 independent experiments. See also Figure S2.

(D) Example of activation markers and PD-1 abundance during CD8 T cell proliferation.

(E and F) Averaged median fluorescence intensity (MFI) of indicated proteins, with error bars representing mean with SEM. For each cell generation of each donor, the fold change is shown with the error bars depicting the mean and 95% confidence interval. Ns, $p > 0.05$; *$p < 0.05$; **$p < 0.01$; ***$p < 0.001$; ****$p < 0.0001$ (two-way ANOVA followed by Bonferroni test). 11–17 donors, 3–5 independent experiments.

(G) A dotted line shows the gate for cells that upregulated TOX after activation. FMO = fluorescence minus one.

(H) Frequency of TOX[up] cells in ctrl or IRF4[KO] cells. ***$p < 0.001$ (Wilcoxon matched pairs). 11 donors, 3 independent experiments.
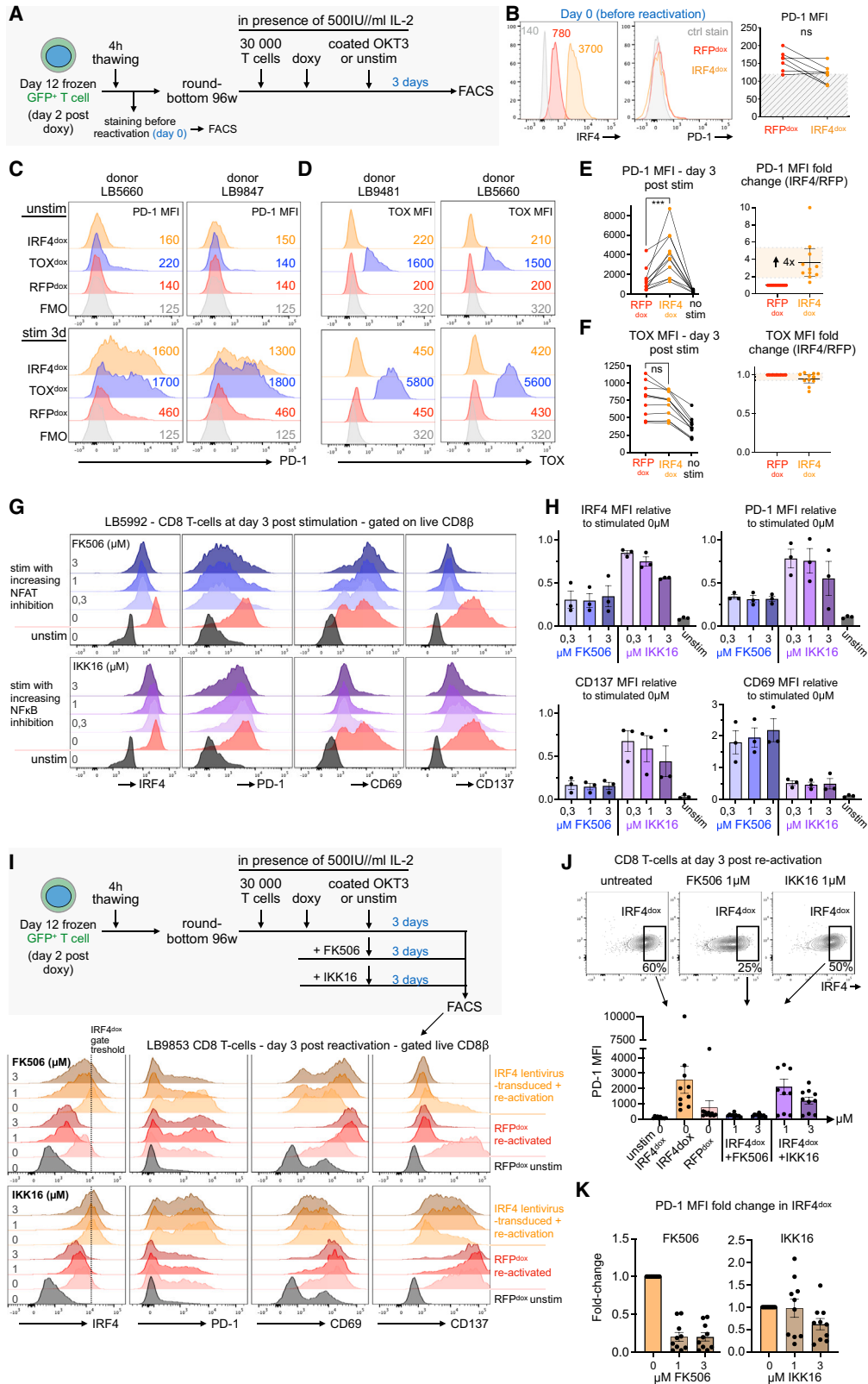
(legend on next page)

we reliably identified "exhausted" CD8 TILs, in which we analyzed IRF4 expression.

Approximately 80% of IRF4+ TILs were PD-1hi cells, suggesting that IRF4 is mainly present in TILs with an exhausted phenotype (Figure 6D). However, 40% of IRF4− cells were also PD-1hi, and overall, 30% of PD-1hi TILs expressed IRF4 (Figures 6D and 6E). Since IRF4 is transiently detectable after TCR activation, this suggests that PD-1hi IRF4+ TILs were recently activated. Indeed, the proportion of CD137+ cells in PD-1hi TILs paralleled the proportion of IRF4+ cells in PD-1hi TILs (Figures 6F–6H). These data show that a fraction of TILs expressing exhaustion markers are also activated. Conversely, an averaged 50% of PD-1hi TILs did not express Ki67, suggesting that these cells were quiescent. Accordingly, very few Ki67− PD-1hi cells expressed IRF4, in contrast to their Ki67+ counterparts (Figures 6I and 6J). However, not all Ki67+ cells expressed IRF4 (Figure 6I). Overall, PD-1hi CD8 TILs are a heterogeneous population of quiescent and activated cells, and IRF4 expression reflects one of these activation states.

High PD-1 and TOX are not solely due to activation and identify dysfunctional TILs

We then assessed PD-1 subsets in CD8 TILs for their ability to produce interferon γ (IFNγ). Upon anti-CD3 activation, fewer PD-1hi TILs produced IFNγ (Figures S6E–S6G). IFNγ production in PD-1hi TILs could be forced with phorbol 12-myristate 13-acetate and ionomycin, but per cell, IFNγ remained lower than in the PD-1neg and PD-1int IFNγ producers (Figures S6H–S6J). Thus, high PD-1 and TOX expression identified less functional TILs, which could reflect exhaustion and/or activation.

To determine whether high PD-1 and TOX expression was solely due to TIL activation state, we compared them to CD8 T cells responding to severe acute respiratory syndrome coronavirus 2 (SARS-CoV-2) infection in the blood of patients with COVID-19 (Figure 6K). High CD38 expression identified virus-activated CD8 T cells with frequent IRF4 and Ki67 expression (Figures 6L–6P). However, PD-1hi cells rarely exceeded 10% of CD38hi cells despite their activation status (Figure 6Q). Besides, among the 8 samples for which enough PD-1hi CD38hi cells were detectable, only 3 had PD-1hi CD38hi expressing TOX levels within the lower range observed in TILs (Figures 6R–6T). Since SARS-CoV-2 activated CD8 T cells were rarely TOXhi PD-1hi, the high expression of PD-1 and TOX in TILs could not solely be attributed to their activation. We conclude that PD-1hi TOXhi CD8 TILs in which IFNγ production is impaired and IRF4 expressed are not solely activated but also exhausted.

DISCUSSION

Our work reports, for the first time, the roles of IRF4 in human CD8 T cells. We showed that IRF4 promotes T cell proliferation and PD-1 expression while restraining T cell effector functions. Transcriptional programs associated with T cell proliferation and effector function were consistently affected by IRF4. Another important finding of our work comes from the unprecedented comparison of CD8 TIL phenotype to activated T cells in patients with COVID-19. This allowed us to conclude that PD-1hi TOXhi TILs, in which IRF4 is partially expressed, are exhausted. The fact that these TILs express PD-1, have low IFNγ production, and are actively cycling (Ki67+) are all attributes that are IRF4 dependent, as reported in this study.

By triggering IRF4 expression either via our inducible lentiviral system or by simple TCR activation, we showed that IRF4 restrains cytokine production and degranulation in CD8 T cells from blood of non-cancerous donors. This regulatory role of IRF4 was not uncovered in studies done in viral acute infection models, as in these models, IRF4 expression is not maintained due to rapid antigen clearance. Consequently, IRF4's role was confined to the naive and effector T cell stage, where IRF4 is required for CD8 T cell differentiation and functions.[27,28] Later work in the chronic viral infection mouse model showed that sustained expression of IRF4 impairs CD8 T cell function and glycolysis and promotes PD-1 expression, thus leading us to conclude that IRF4 promotes T cell exhaustion.[30] Our findings are in line with IRF4 impairing T cell function and promoting PD-1 expression, but we show that simple T cell activation mimics these attributes of exhaustion in an IRF4-dependent manner. Regulatory mechanisms of T cell functions are thus systemically at work to adapt T cell activity against an antigen independently of T cell exhaustion and may share some transcriptional regulation with exhaustion since downregulated genes during T cell exhaustion were also downregulated in IRF4-overexpressing T cells.

Our work suggests that part of the low effector functions conventionally attributed to exhaustion could derive from simple

---

Figure 4. Abundance of IRF4 exacerbates PD-1 expression and requires NFAT activity

(A) Experiment overview.

(B) Abundance of IRF4 and PD-1 after CD8 T cell thawing, before reactivation. Gray histograms represent control staining (control isotype for IRF4, or FMO for PD-1).

(C and D) Representative examples of PD-1 (C) and TOX (D) abundance 3 days after reactivation (stim 3d) or not (unstim).

(E and F) MFI for each donor. The no-stim control data shown were the same in RFPdox or IRF4dox T cells. The fold change of PD-1 (E) or TOX (F) MFI is shown with the error bars depicting the mean value and 95% confidence interval (orange area) (11 donors, 3 independent experiments). ***$p < 0.001$ (Wilcoxon matched pairs). See also Figure S3.

(G) Representative flow cytometry plots of activation markers for cells treated with TCR signaling inhibitors.

(H) MFI fold change of the indicated proteins.

(I) Experiment overview and representative flow cytometry plots of RFPdox (red) or IRF4dox (orange) activation markers after treatment or no treatment with the indicated TCR signaling inhibitor.

(J) Gating strategy on IRF4dox cells to quantify PD-1 MFI.

(K) The fold change of PD-1 MFI is plotted for each IRF4dox sample treated with inhibitors relative to untreated activated IRF4dox cells (10 donors, 2 independent experiments).

Error bars in (H), (J), and (K) show mean + SEM, and each dot represents one sample.
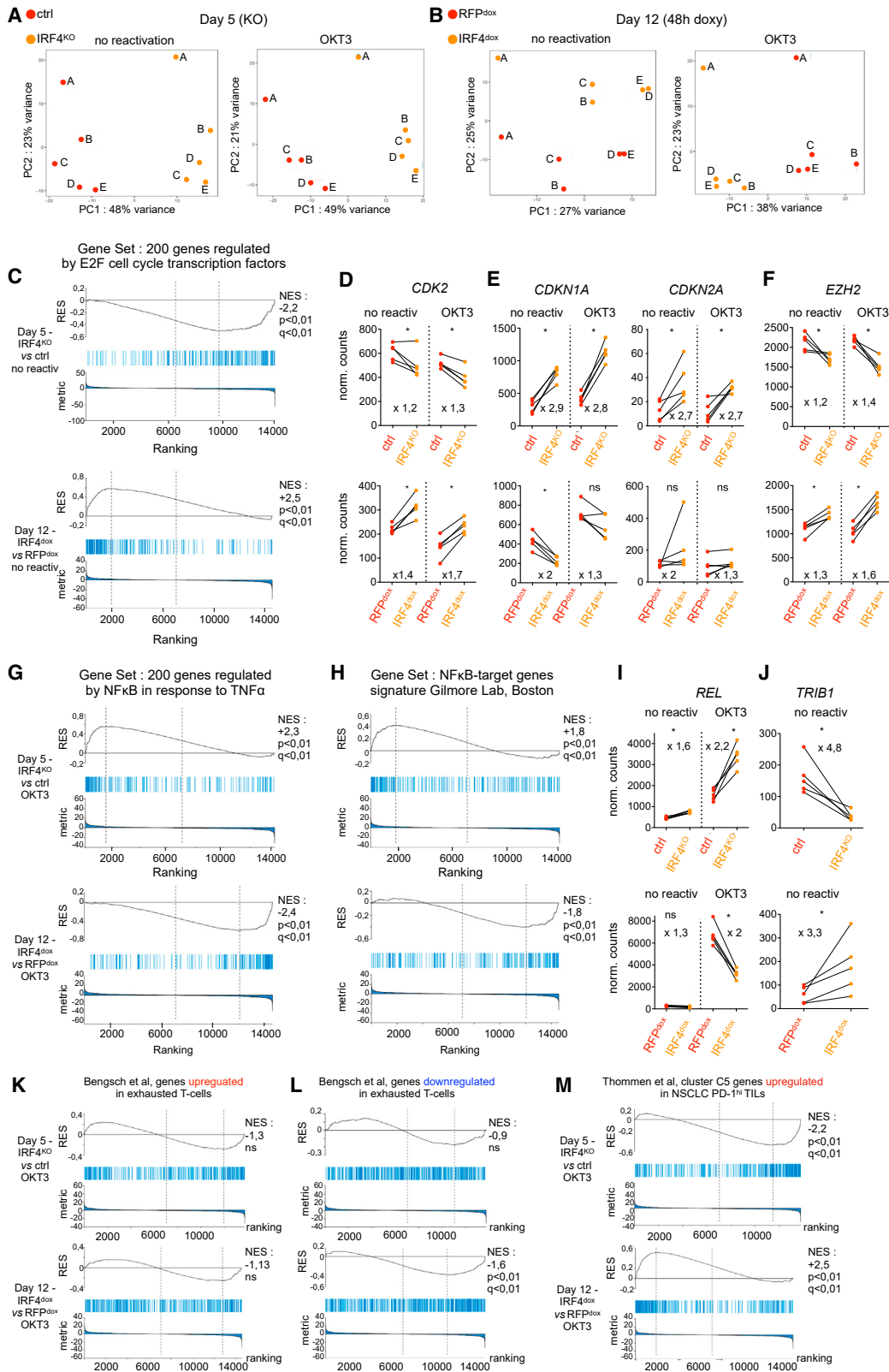
(legend on next page)

IRF4 upregulation after T cell activation. Similarly, when exhausted CD8 T cells from chronically infected mice rest into antigen-free mice, they partially recover effector functions and have decreased PD-1 expression.[26] Similarly, human T cells transduced with a chimeric antigen receptor (CAR) that triggers tonic antigen-independent signaling have improved functionality after transient rest.[37] Interestingly, the same research group showed that tonically activated CAR T cells also have improved IFNγ secretion if IRF4 expression is knocked out.[38] Altogether, this highlights a direct link between T cell activation, IRF4 expression, and T cell function.

Our transcriptomic analysis revealed that IRF4 impairs the expression of NF-κB-regulated genes, which could explain partially why IRF4 repressed cytokine production and transcription of the corresponding genes. In a mouse model of melanoma, CD8 TILs overexpress the protein A20, a NF-κB pathway inhibitor, and have impaired IFNγ and tumor necrosis factor alpha (TNF-α) production. Deletion of A20 improved cytokine production and tumor control. This was associated to improved nuclear translocation of RelA and c-Rel.[39] Our data did not extend these findings to IRF4 in human CD8 T cells, as we did not observe impaired RelA translocation by IRF4. Whether IRF4 inhibits translocation of c-Rel was not investigated, since c-Rel is not rapidly mobilized by TCR signals due to its association with IκBβ40. Furthermore, non-naïve c-$Rel^{-/-}$ T cells have intact cytokine production upon 4-h activation.[40] Therefore, it is likely that IRF4 affects the expression of NF-κB-regulated genes by transcriptional regulatory mechanisms rather than through faulty NF-κB signaling. Specifically, the NF-κB1-RelA complex binds to the κB *cis* motif on the IFNγ gene to enhance its expression.[41,42] Whether IRF4 hinders this binding warrants further investigation.

NFAT proteins interact with structurally unrelated Jun-Fos (AP-1) transcription factors to form cooperative NFAT-AP-1 complexes that are critical for the induction of cytokine genes and other activation-associated genes. Several pieces of evidence point toward altered NFAT-AP-1 activity by IRF4. We observed that *REL* (c-Rel) and *CSF2* (GM-CSF [granulocyte-macrophage colony-stimulating factor]) expression was impaired by IRF4 upon TCR activation. Upregulation of c-Rel is RelA independent and instead requires NFAT-AP-1 activity.[43,44] GM-CSF expression also requires NFAT-AP-1 activity.[45,46] In chronically activated CAR T cells, IRF4 abundance leads to the formation of c-Jun-IRF4 complexes rather than activating c-Jun-c-Fos (AP-1) complexes on DNA. Besides, c-Jun-c-Fos binding sites are instead occupied by JunB-BATF-IRF4 complexes.[38] Upon c-Jun overexpression, these complexes are displaced from their AP-1-IRF element (AICE), which leads to

enhancement of CAR T cell function such as IFNγ secretion, and this effect can be reproduced by IRF4 KO.[38] Such a mechanism could also account for the repression of cytokine production by IRF4 reported in our work.

The role of IRF4 for human CD8 T cell proliferation was probably our most expected finding, since, during both an acute and a chronic viral infection, IRF4 is required for CD8 T cell expansion.[27,28,30] It is worth noting that, in these studies, IRF4 is already deficient in naive T cells and thus appears to be required for T cell expansion during effector differentiation. Our experiments used a mixture of naive and non-naive CD8 T cells isolated from human blood. We observed a proliferation defect in IRF4^KO T cells after anti-CD3 activation, irrespectively of CD28 co-stimulation. Since anti-CD3 activation without co-stimulation fails to induce proliferation of naive T cells,[47] our results indicate that IRF4, which was known to support murine T cell proliferation from the naive to the effector stage, also support memory T cells proliferation in humans. Similarly, a mouse model in which partial KO of IRF4 is induced once memory T cells are formed showed that $Irf4^{+/-}$ memory T cells have reduced proliferation upon reactivation.[48]

Our transcriptomic analysis suggests that IRF4 promotes T cell proliferation by favoring progression in the cell cycle. Precisely, IRF4 could control the G1/S phase transition, as the cell cycle gene set upregulated by IRF4 is involved in this process. Previous data in mice support this notion, as $Irf4^{-/-}$ CD8 T-cells responding to acute viral infection have lower incorporation of the thymidine analog bromodeoxyuridine and upregulated expression of the *Cdkn1a* and *Cdkn2a* inhibitors of G1/S phase transition.[28] Similarly, we showed that IRF4 upregulates *CDK2*, which promotes G1/S phase transition by associating with cyclin E, and that IRF4 downregulates *CDKN1A* and *CDKN2A* inhibitors of cell cycle progression. IRF4 also upregulated *EZH2*, a transcription factor that promotes CD8 T cell expansion and inhibits *CDKN2A*.[34,49] Interestingly, EZH2 is a target of BATF-IRF4 and is upregulated in BATF-overexpressing CAR T cells. Overexpression of a mutant form of BATF that cannot interact with IRF4 leads to defective CAR T cell expansion.[50] Thus, regulation of cell cycle genes in favor of T cell proliferation by IRF4 was probably the result of collaboration with its transcriptional partner BATF. This could also apply to human TILs *in vivo*, since we found that IRF4 promotes the expression of cell cycle and proliferation genes that are overexpressed in NSCLC PD-1^hi TILs.[11]

While lentiviral induction of IRF4 drove expression of cell cycle genes, it did not result in improved T cell proliferation upon 3-day reactivation of these IRF4-overexpressing cells. In mice, CD8

Figure 5. IRF4 regulates cell cycle gene expression and impairs NF-κB-regulated gene expression

(A and B) Principal-component analysis (PCA) plots of 16,493 genes expressed in control and IRF4^KO cells (A) or 18,261 genes expressed in RFP^dox and IRF4^dox cells (B) that were reactivated or not for 5 h. Each dot on the PCA represents a sample from the indicated donor.

(C) GSEA on gene set Hallmark_E2F_Target.

(D–F) Selected gene expression values for each donor in the indicated condition.

(G and H) GSEA on gene set Hallmark_TNFA_signaling_by_NF-κB (G) and gene set NF-κB_target_genes signature from the Gilmore lab (H).

(I and J) Selected gene expression values for each donor in the indicated condition. *adjusted $p < 0.05$; ns, adjusted $p > 0.05$ (DESeq2 paired test).

(K and L) GSEA on differentially expressed genes in exhausted T cells as described previously.[36]

(M) GSEA on a cluster of genes upregulated in PD-1^high TILs from NSCLC as described previously.[11] See also Figure S4, Tables S1 and S2, and STAR Methods for GSEA settings.

A FMO LB9256 TILs | non-cancerous LB9335 blood | cancer patient LB9189 blood | cancer patient LB9189 TILs

B FMO LB9256 TILs | non-cancerous LB9335 blood | cancer patient LB9189 blood | cancer patient LB9189 TILs

C CD8β TILs of patient LB9189

D LB9256 TILs CD8β — % PD1hi in indicated IRF4 subset

E % IRF4+ in indicated PD-1 subset

F LB9256 TILs CD8β — % CD137+ in indicated IRF4 subset

G % CD137+ in indicated PD-1 subset

H spearman r = 0,95; slope = 0,89; r²=0,89

I LB9256 TILs CD8β — % IRF4+ in indicated Ki67 subset

J % Ki67+ in indicated PD-1 subset

K frozen cells (non-cancer blood, COVID19 blood, solid tumor)

L non-cancerous - LB9335 blood | COVID19 patient

M % of indicated CD38 subset in blood

N % Ki67+ in indicated subset | % IRF4+ in indicated subset

O % Ki67+ in indicated subset

P % IRF4+ in indicated subset

Q TILs LB9257 CD8β | COVID-19 LB9342 CD38hi | COVID-19 LB9309 CD38hi

R % of PD-1hi in indicated subset

S CD8β TILs — MFI

T TOX MFI in indicated subset

(legend on next page)

T cells receiving a weak TCR stimulus causing low IRF4 expression benefit from IRF4 retroviral transduction for proliferation. But when a higher amount of IRF4 is synthetized after stronger TCR stimuli, supplemental amounts of IRF4 supplied by retroviral transduction barely improve T cell proliferation.[28] Consequently, it is possible that we did not observe any positive effect on cell proliferation by overexpressing IRF4 because endogenous amounts of IRF4 synthetized after TCR reactivation were enough for efficient cell proliferation.

However, we did observe that overexpression of IRF4 was able to increase PD-1 expression and that there was a dose-dependent effect of IRF4 on resulting levels of PD-1. The fact that TCR-induced amounts of IRF4 can be on one side sufficient for efficient T cell proliferation, but, on the other side, limiting for PD-1 expression suggests uncoupled regulation of T cell proliferation and PD-1 expression by IRF4. Indeed, complete lack of PD-1 was observed on the surface of IRF4[KO] T cells, even the proliferating ones. Insights into transcriptional control of gene expression by IRF4 may explain these observations. In association with its main transcriptional partner BATF, IRF4 binds to AICEs on its target genes.[51,52] In mouse CD4 T cells, it has been shown that, depending on nucleotide context of type 2 AICEs, their affinity for IRF4-BATF changes.[53] High-affinity AICEs are contained in genes whose expression is induced by IRF4 and BATF even when IRF4 levels are low. Low-affinity AICEs are contained in genes whose expression is induced only when sufficient amounts of IRF4 are synthetized.[53] Consequently, it is likely that the genes regulated by IRF4 for cell proliferation are genes with high-affinity AICE motifs. Expression of these genes changes proportionally to the amount of IRF4 due to the high sensitivity of high-affinity AICEs. This would explain the close relationship between the amount of IRF4 synthesized and the resulting level of proliferation and why, when a given endogenous level of IRF4 is reached, overexpressing IRF4 does not improve proliferation anymore, as our data and others have shown. Conversely, the *PDCD1* gene could contain a low-affinity AICE motif that accommodates IRF4 recruitment only in the presence of high amounts of IRF4, hence the fact that lentiviral transduction of IRF4 amplified PD-1 expression. This hypothesis may, however, not hold true in every situation, since we also found samples with increased PD-1 levels without increased *PDCD1* mRNA levels. Interestingly, TOX has been shown to increase surface PD-1 levels in human CD8 T cells by facilitating endocytic recycling of PD-1, while PD-1 gene expression was unchanged.[54] However, we showed that IRF4 overexpression did not change TOX levels. How IRF4 overexpression increases PD-1 protein levels warrants further investigation.

While IRF4 and BATF could collaborate on AICE to exacerbate PD-1 expression, our data also showed that IRF4 collaborates with NFAT for PD-1 gene transcription. NFAT is known to co-regulate gene transcription with IRF4 in human CD4 T cells.[55,56] Furthermore, chromatin immunoprecipitation sequencing (ChIP-seq) data in mouse CD8 T cells showed that BATF, IRF4, and NFAT bind together to *Pdcd1* during viral infection.[30] Murine NFAT is known to drive *Pdcd1* expression,[57,58] and correspondingly, our data demonstrate that IRF4 requires NFAT activity for PD-1 expression. In turn, our data show that NFAT requires IRF4 activity for the amplification of PD-1 expression. Indeed, while PD-1 could be detected before cell division, further upregulation of PD-1 was proportional to IRF4 expression as T cells proliferated. Our data also showed that NF-κB had less importance for PD-1 expression than NFAT or IRF4, which is compatible with our observation that IRF4 represses NF-κB-regulated genes while promoting PD-1 expression.

In silico analysis of public ChIP-seq data reported binding of IRF4 and NFAT-1 to the *Tox* locus in mouse T cells.[22] In mice, NFAT is required for TOX expression by CD8 T cells.[13,22] Similarly to PD-1, we showed that sustained TOX expression required IRF4, which aligns with IRF4 binding to the *Tox* locus in mice. Thus, NFAT also requires IRF4 to mediate TOX upregulation. Whether high, sustained TOX levels leading to T cell exhaustion require IRF4 as well warrants further investigation.

The transcription factor IRF4 displays several properties that allow its exquisite control of T cell response. Indeed, there is a direct connection between TCR activation strength and the

---

Figure 6. IRF4 is expressed in human CD8 TILs displaying exhaustion and activation markers

(A and B) Gating strategy to stratify CD8 T cells in 3 subsets based on FMO control and protein signal measured in non-cancerous and cancerous situations.

(C) Example showing that TOX[hi] CD8 TILs (green) fall into the PD-1^{hi} gate (top) and that the PD-1^{hi} CD8 TILs (pink) fall into the TOX^{hi} gate (bottom).

(D–F) Gating strategy to identify IRF4^{+} cells (D) or CD137^{+} (F) cells in CD8 TILs (left) and proportion of PD-1^{hi} (D) or CD137^{+} (F) cells in IRF4^{+} or IRF4^{−} cell subsets (right).

(E–G) Proportion of IRF4^{+} (E) or CD137^{+} (G) CD8 T cells in the indicated PD-1 subset from blood and tumor.

(H) Correlation between CD137 and IRF4 abundance in PD-1^{hi} CD8 TILs.

(I) Gating strategy to identify Ki67^{+} cells in CD8 T cells (left) and proportion of IRF4^{+} cells in PD-1^{hi} Ki67^{−} or PD-1^{hi} Ki67^{+} CD8 TILs (right).

(J) Proportion of Ki67^{+} CD8 T cells in the indicated PD-1 subset from blood and tumor. **$p < 0.01$ (Wilcoxon matched pairs) for (C), (F), and (I) and ****$p < 0.0001$ (Spearman test) for (H).

(K) Experiment overview to compare phenotype of CD8 T cells from blood of patients with COVID-19 to CD8 TILs from patients with ovarian cancer.

(L) Gating strategy to stratify CD8 T cells based on CD38 detection.

(M) Proportion of the indicated CD38 subset in CD8 T cells from blood (ICU, intensive care unit).

(N) Proportion of Ki67^{+} (left) or IRF4^{+} cells (right) within the indicated CD38 subset in blood CD8 T cells compared with PD-1^{hi} TILs.

(O and P) Proportion of Ki67^{+} (O) or IRF4^{+} cells (P) in the indicated subset of CD8 T cells from patients with COVID-19.

(Q) Example of PD-1 stratification in CD8 TILs or in CD38^{hi} CD8 T cells from COVID-19 samples.

(R) Proportion of PD-1^{hi} cells within the indicated CD38 subset in blood of patients with COVID-19 compared with CD8 TILs.

(S) Example of patients with COVID-19 in which the CD38^{hi} PD-1^{hi} cells had similar TOX levels as PD-1^{hi} TILs.

(T) TOX MFI in the indicated CD8 T cell subsets.

Data are from 3 (A–K) or 2 (L–S) independent experiments. Each dot represents one sample. *$p < 0.05$, **$p < 0.01$, ***$p < 0.001$ (Kruskal-Wallis test followed by Dunn test).

abundance of IRF4, and the *cis* elements recognized by IRF4 exist with different affinities that respond to different doses of IRF4.[27,53] This places IRF4 at the core of a circuit in which the input signal is integrated by IRF4 so that the output signal produced by a T cell is correctly adjusted. Illustrating this notion, 95% of genes that are differentially expressed between a T cell activated with a low-affinity peptide and a high-affinity peptide are under the control of IRF4.[27] This illustrates how important IRF4 could be to calibrate a CD8 T cell response according to the nature of an antigen. This is of outmost importance, since an exacerbated immune response is detrimental to the organism. For instance, *PD-1*$^{-/-}$ or *PD-L1*$^{-/-}$ mice infected with a high viral load of LCMV succumb to the infection within a week, which is not observed following infection with a low viral load.[59,60] The mortality resulting from the infection is correlated with abnormally high levels of IFNγ and TNF-α in the serum of *PD-1*$^{-/-}$ mice and the exaggerated presence of lesions in infected tissues and is CD8 T cell dependent.[59,61] Our work shows that, in human CD8 T cells, IRF4 promotes the expression of PD-1 and attenuates the function of the CD8 T cells whose proliferation is favored by IRF4. By doing so, IRF4 would allow tempering an immune response that could otherwise be detrimental if a massive pool of clonally expanded T cells had unleashed activity.

From a therapeutic view, it is conceivable that IRF4 expression in human CAR T cells could be finely modulated to achieve different goals. Inducing moderate expression of IRF4 would limit its effect on CAR T cell function while promoting their proliferation, thus maximizing their activity in the tumor. Conversely, overexpressing IRF4 would also increase the number of CAR T cells but mitigates the amount of inflammatory cytokines they produce and their lytic activity. This strategy would limit major inflammatory side effects that are often caused by CAR T cell administration in patients with cancer.[62]

Limitations of the study
Our study shows that IRF4 is necessary for T cell proliferation. However, increasing its levels did not impact proliferation. We reached these conclusions through fluorescent cell tracker dilution experiments, allowing us to calculate various proliferation metrics. While these metrics were lower in cells lacking IRF4, resulting in reduced T cell yield, proliferation metrics remain unchanged in cells overexpressing IRF4. However, we could not estimate the total T cell yield due to the fact that overexpression of IRF4 with doxycycline was variable and limited to around 40% of cells. It remains plausible that IRF4 overexpression could promote T cell expansion despite similar proliferation rates, possibly by reducing death, as observed in mouse T cells.[27,28]

We found that increased PD-1 levels in IRF4-overexpressing T cells were not necessarily due to elevated *PDCD1* mRNA levels. Our analysis was limited to a 45-h activation time point to corroborate our findings with our CRISPR-Cas9 system. Analyzing multiple and earlier time points than 45 h could have yielded different results.

We used blood CD8 T cells from non-cancerous donors that display a transcriptional and epigenetic landscape that differs from those found in exhausted TILs. Whether the effects produced by IRF4 in our work would apply to human TILs remains uncertain. However, it is remarkable that cell-cycle and proliferation genes upregulated by IRF4 are overexpressed in PD-1^{hi} TILs and that IRF4 overexpression downregulated core exhaustion genes that are also found to be downregulated in mouse and human exhausted T cells.

STAR★METHODS

Detailed methods are provided in the online version of this paper and include the following:

- KEY RESOURCES TABLE
- RESOURCE AVAILABILITY
  - Lead contact
  - Materials availability
  - Data and code availability
- EXPERIMENTAL MODEL AND STUDY PARTICIPANT DETAILS
- METHOD DETAILS
  - Cell culture and media
  - Tumor and peripheral blood mononuclear cells isolation from patients
  - CD8 T-cell isolation from non-cancerous donors
  - Plasmids and lentiviral production
  - CD8 T cell lentiviral transduction and doxycycline induction
  - CRISPR/Cas9
  - Cytokine production assay
  - Degranulation assay
  - Proliferation assay and concomitant measurement of activation markers expression
  - Extracellular and intracellular stainings for flow cytometry
  - NF-κB translocation assay
  - Intracellular staining prior to RNA extraction
  - RNA extraction from fixed and permeabilized cells
  - RNAseq libraries construction, sequencing, and analysis
  - RNAseq data analysis and GSEA
  - Preparation of RNA for RT-qPCR of *IFNG, TNFA, CSF2 and PDCD1*
  - RT-qPCR for *IFNG*, *TNFA*, *CSF2* and *PDCD1*
- QUANTIFICATION AND STATISTICAL ANALYSIS

SUPPLEMENTAL INFORMATION

Supplemental information can be found online at https://doi.org/10.1016/j.celrep.2024.114401.

AUTHOR CONTRIBUTIONS

T.H. and P.v.d.B. wrote the manuscript. T.H., D.N., and P.v.d.B. conceived the project. T.H., C.D., and D.N. conducted the experiments. A.B. performed RNA-seq library construction and quantitative real-time PCR. C.V. performed the bioinformatic analyses and T.H. the analyses with Qlucore. F.S.d.O.

REFERENCES

1. Angelosanto, J.M., Blackburn, S.D., Crawford, A., and Wherry, E.J. (2012). Progressive Loss of Memory T Cell Potential and Commitment to Exhaustion during Chronic Viral Infection. J. Virol. 86, 8161–8170. https://doi.org/10.1128/jvi.00889-12.

2. Im, S.J., Hashimoto, M., Gerner, M.Y., Lee, J., Kissick, H.T., Burger, M.C., Shan, Q., Hale, J.S., Lee, J., Nasti, T.H., et al. (2016). Defining CD8+ T cells that provide the proliferative burst after PD-1 therapy. Nature 537, 417–421. https://doi.org/10.1038/nature19330.

3. Utzschneider, D.T., Charmoy, M., Chennupati, V., Pousse, L., Ferreira, D.P., Calderon-Copete, S., Danilo, M., Alfei, F., Hofmann, M., Wieland, D., et al. (2016). T Cell Factor 1-Expressing Memory-like CD8+ T Cells Sustain the Immune Response to Chronic Viral Infections. Immunity 45, 415–427. https://doi.org/10.1016/j.immuni.2016.07.021.

4. Utzschneider, D.T., Gabriel, S.S., Chisanga, D., Gloury, R., Gubser, P.M., Vasanthakumar, A., Shi, W., and Kallies, A. (2020). Early precursor T cells establish and propagate T cell exhaustion in chronic infection. Nat. Immunol. 21, 1256–1266. https://doi.org/10.1038/s41590-020-0760-z.

5. Miller, B.C., Sen, D.R., Al Abosy, R., Bi, K., Virkud, Y.V., LaFleur, M.W., Yates, K.B., Lako, A., Felt, K., Naik, G.S., et al. (2019). Subsets of exhausted CD8+ T cells differentially mediate tumor control and respond to checkpoint blockade. Nat. Immunol. 20, 326–336. https://doi.org/10.1038/s41590-019-0312-6.

6. Siddiqui, I., Schaeuble, K., Chennupati, V., Fuertes Marraco, S.A., Calderon-Copete, S., Pais Ferreira, D., Carmona, S.J., Scarpellino, L., Gfeller, D., Pradervand, S., et al. (2019). Intratumoral Tcf1 + PD-1 + CD8 + T Cells with Stem-like Properties Promote Tumor Control in Response to Vaccination and Checkpoint Blockade Immunotherapy. Immunity 50, 195–211.e10. https://doi.org/10.1016/j.immuni.2018.12.021.

7. Beltra, J.C., Manne, S., Abdel-Hakeem, M.S., Kurachi, M., Giles, J.R., Chen, Z., Casella, V., Ngiow, S.F., Khan, O., Huang, Y.J., et al. (2020). Developmental Relationships of Four Exhausted CD8+ T Cell Subsets Reveals Underlying Transcriptional and Epigenetic Landscape Control Mechanisms. Immunity 52, 825–841.e8. https://doi.org/10.1016/j.immuni.2020.04.014.

8. McLane, L.M., Abdel-Hakeem, M.S., and Wherry, E.J. (2019). CD8 T Cell Exhaustion During Chronic Viral Infection and Cancer. Annu. Rev. Immunol. 37, 457–495. https://doi.org/10.1146/annurev-immunol-041015-055318.

9. Ahmadzadeh, M., Johnson, L.A., Heemskerk, B., Wunderlich, J.R., Dudley, M.E., White, D.E., and Rosenberg, S.A. (2009). Tumor antigen-specific CD8 T cells infiltrating the tumor express high levels of PD-1 and are functionally impaired. Blood 114, 1537–1544. https://doi.org/10.1182/blood-2008-12-195792.

10. Matsuzaki, J., Gnjatic, S., Mhawech-Fauceglia, P., Beck, A., Miller, A., Tsuji, T., Eppolito, C., Qian, F., Lele, S., Shrikant, P., et al. (2010). Tumor-infiltrating NY-ESO-1-specific CD8+ T cells are negatively regulated by LAG-3 and PD-1 in human ovarian cancer. Proc. Natl. Acad. Sci. USA 107, 7875–7880. https://doi.org/10.1073/pnas.1003345107.

11. Thommen, D.S., Koelzer, V.H., Herzig, P., Roller, A., Trefny, M., Dimeloe, S., Kiialainen, A., Hanhart, J., Schill, C., Hess, C., et al. (2018). A transcriptionally and functionally distinct pd-1+ cd8+ t cell pool with predictive potential in non-small-cell lung cancer treated with pd-1 blockade. Nat. Med. 24, 994–1004. https://doi.org/10.1038/s41591-018-0057-z.

12. Alfei, F., Kanev, K., Hofmann, M., Wu, M., Ghoneim, H.E., Roelli, P., Utzschneider, D.T., von Hoesslin, M., Cullen, J.G., Fan, Y., et al. (2019). TOX reinforces the phenotype and longevity of exhausted T cells in chronic viral infection. Nature 571, 265–269. https://doi.org/10.1038/s41586-019-1326-9.

13. Khan, O., Giles, J.R., McDonald, S., Manne, S., Ngiow, S.F., Patel, K.P., Werner, M.T., Huang, A.C., Alexander, K.A., Wu, J.E., et al. (2019). TOX transcriptionally and epigenetically programs CD8+ T cell exhaustion. Nature 571, 211–218. https://doi.org/10.1038/s41586-019-1325-x.

14. Scott, A.C., Dündar, F., Zumbo, P., Chandran, S.S., Klebanoff, C.A., Shakiba, M., Trivedi, P., Menocal, L., Appleby, H., Camara, S., et al. (2019). TOX is a critical regulator of tumour-specific T cell differentiation. Nature 571, 270–274. https://doi.org/10.1038/s41586-019-1324-y.

15. Sekine, T., Perez-Potti, A., Nguyen, S., Gorin, J.B., Wu, V.H., Gostick, E., Llewellyn-Lacey, S., Hammer, Q., Falck-Jones, S., Vangeti, S., et al. (2020). TOX is expressed by exhausted and polyfunctional human effector memory CD8+ T cells. Sci. Immunol. 5, eaba7918-15. https://doi.org/10.1126/sciimmunol.aba7918.

16. Tirosh, I., Izar, B., Prakadan, S.M., Wadsworth, M.H., Treacy, D., Trombetta, J.J., Rotem, A., Rodman, C., Lian, C., Murphy, G., et al. (2016). Dissecting the multicellular ecosystem of metastatic melanoma by single-cell RNA-seq. Science (1979) 352, 189–196. https://doi.org/10.1126/science.aad0501.

17. Zheng, C., Zheng, L., Yoo, J.K., Guo, H., Zhang, Y., Guo, X., Kang, B., Hu, R., Huang, J.Y., Zhang, Q., et al. (2017). Landscape of Infiltrating T Cells in Liver Cancer Revealed by Single-Cell Sequencing. Cell 169, 1342–1356.e16. https://doi.org/10.1016/j.cell.2017.05.035.

18. Guo, X., Zhang, Y., Zheng, L., Zheng, C., Song, J., Zhang, Q., Kang, B., Liu, Z., Jin, L., Xing, R., et al. (2018). Global characterization of T cells in non-small-cell lung cancer by single-cell sequencing. Nat. Med. 24, 978–985. https://doi.org/10.1038/s41591-018-0045-3.

19. Savas, P., Virassamy, B., Ye, C., Salim, A., Mintoff, C.P., Caramia, F., Salgado, R., Byrne, D.J., Teo, Z.L., Dushyanthen, S., et al. (2018). Single-cell profiling of breast cancer T cells reveals a tissue-resident memory subset associated with improved prognosis. Nat. Med. 24, 986–993. https://doi.org/10.1038/s41591-018-0078-7.

20. Zhang, L., Yu, X., Zheng, L., Zhang, Y., Li, Y., Fang, Q., Gao, R., Kang, B., Zhang, Q., Huang, J.Y., et al. (2018). Lineage tracking reveals dynamic relationships of T cells in colorectal cancer. Nature 564, 268–272. https://doi.org/10.1038/s41586-018-0694-x.

21. Li, H., van der Leun, A.M., Yofe, I., Lubling, Y., Gelbard-Solodkin, D., van Akkooi, A.C.J., van den Braber, M., Rozeman, E.A., Haanen, J.B.A.G., Blank, C.U., et al. (2019). Dysfunctional CD8 T Cells Form a Proliferative, Dynamically Regulated Compartment within Human Melanoma. Cell 176, 775–789.e18. https://doi.org/10.1016/j.cell.2018.11.043.

22. Yao, C., Sun, H.W., Lacey, N.E., Ji, Y., Moseman, E.A., Shih, H.Y., Heuston, E.F., Kirby, M., Anderson, S., Cheng, J., et al. (2019). Single-cell RNA-seq reveals TOX as a key regulator of CD8+ T cell persistence in chronic infection. Nat. Immunol. 20, 890–901. https://doi.org/10.1038/s41590-019-0403-4.

23. Blackburn, S.D., Shin, H., Haining, W.N., Zou, T., Workman, C.J., Polley, A., Betts, M.R., Freeman, G.J., Vignali, D.A.A., and Wherry, E.J. (2009). Coregulation of CD8+ T cell exhaustion by multiple inhibitory receptors during chronic viral infection. Nat. Immunol. 10, 29–37. https://doi.org/10.1038/ni.1679.

24. Fourcade, J., Sun, Z., Benallaoua, M., Guillaume, P., Luescher, I.F., Sander, C., Kirkwood, J.M., Kuchroo, V., and Zarour, H.M. (2010). Upregulation of Tim-3 and PD-1 expression is associated with tumor antigen-specific CD8+ T cell dysfunction in melanoma patients. J. Exp. Med. 207, 2175–2186. https://doi.org/10.1084/jem.20100637.

25. Thommen, D.S., Schreiner, J., Müller, P., Herzig, P., Roller, A., Belousov, A., Umana, P., Pisa, P., Klein, C., Bacac, M., et al. (2015). Progression of lung cancer is associated with increased dysfunction of T cells defined by coexpression of multiple inhibitory receptors. Cancer Immunol. Res. *3*, 1344–1354. https://doi.org/10.1158/2326-6066.CIR-15-0097.

26. Abdel-Hakeem, M.S., Manne, S., Beltra, J.C., Stelekati, E., Chen, Z., Nzingha, K., Ali, M.A., Johnson, J.L., Giles, J.R., Mathew, D., et al. (2021). Epigenetic scarring of exhausted T cells hinders memory differentiation upon eliminating chronic antigenic stimulation. Nat. Immunol. *22*, 1008–1019. https://doi.org/10.1038/s41590-021-00975-5.

27. Man, K., Miasari, M., Shi, W., Xin, A., Henstridge, D.C., Preston, S., Pellegrini, M., Belz, G.T., Smyth, G.K., Febbraio, M.A., et al. (2013). The transcription factor IRF4 is essential for TCR affinity-mediated metabolic programming and clonal expansion of T cells. Nat. Immunol. *14*, 1155–1165. https://doi.org/10.1038/ni.2710.

28. Yao, S., Buzo, B.F., Pham, D., Jiang, L., Taparowsky, E.J., Kaplan, M.H., and Sun, J. (2013). Interferon regulatory factor 4 sustains CD8+ T cell expansion and effector differentiation. Immunity *39*, 833–845. https://doi.org/10.1016/j.immuni.2013.10.007.

29. Wu, J., Zhang, H., Shi, X., Xiao, X., Fan, Y., Minze, L.J., Wang, J., Ghobrial, R.M., Xia, J., Sciammas, R., et al. (2017). Ablation of Transcription Factor IRF4 Promotes Transplant Acceptance by Driving Allogenic CD4+ T Cell Dysfunction. Immunity *47*, 1114–1128.e6. https://doi.org/10.1016/j.immuni.2017.11.003.

30. Man, K., Gabriel, S.S., Liao, Y., Gloury, R., Preston, S., Henstridge, D.C., Pellegrini, M., Zehn, D., Berberich-Siebelt, F., Febbraio, M.A., et al. (2017). Transcription Factor IRF4 Promotes CD8+ T Cell Exhaustion and Limits the Development of Memory-like T Cells during Chronic Infection. Immunity *47*, 1129–1141.e5. https://doi.org/10.1016/j.immuni.2017.11.021.

31. Leitner, J., Kuschei, W., Grabmeier-Pfistershammer, K., Woitek, R., Kriehuber, E., Majdic, O., Zlabinger, G., Pickl, W.F., and Steinberger, P. (2010). T cell stimulator cells, an efficient and versatile cellular system to assess the role of costimulatory ligands in the activation of human T cells. J. Immunol. Methods *362*, 131–141. https://doi.org/10.1016/j.jim.2010.09.020.

32. Hrvatin, S., Deng, F., O'Donnell, C.W., Gifford, D.K., and Melton, D.A. (2014). MARIS: Method for Analyzing RNA following Intracellular Sorting. PLoS ONE *9*, e89459. https://doi.org/10.1371/journal.pone.0089459.

33. Kent, L.N., and Leone, G. (2019). The broken cycle: E2F dysfunction in cancer. Nat. Rev. Cancer *19*, 326–338. https://doi.org/10.1038/s41568-019-0143-7.

34. Chen, G., Subedi, K., Chakraborty, S., Sharov, A., Lu, J., Kim, J., Mi, X., Wersto, R., Sung, M.H., and Weng, N.P. (2018). Ezh2 regulates activation-induced CD8+ T cell cycle progression via repressing Cdkn2a and Cdkn1c expression. Front. Immunol. *9*, 549. https://doi.org/10.3389/fimmu.2018.00549.

35. Rome, K.S., Stein, S.J., Kurachi, M., Petrovic, J., Schwartz, G.W., Mack, E.A., Uljon, S., Wu, W.W., DeHart, A.G., McClory, S.E., et al. (2020). Trib1 regulates T cell differentiation during chronic infection by restraining the effector program. J. Exp. Med. *217*, e20190888. https://doi.org/10.1084/jem.20190888.

36. Bengsch, B., Ohtani, T., Khan, O., Setty, M., Manne, S., O'Brien, S., Gherardini, P.F., Herati, R.S., Huang, A.C., Chang, K.M., et al. (2018). Epigenomic-Guided Mass Cytometry Profiling Reveals Disease-Specific Features of Exhausted CD8 T Cells. Immunity *48*, 1029–1045.e5. https://doi.org/10.1016/j.immuni.2018.04.026.

37. Weber, E.W., Parker, K.R., Sotillo, E., Lynn, R.C., Anbunathan, H., Lattin, J., Good, Z., Belk, J.A., Daniel, B., Klysz, D., et al. (2021). Transient rest restores functionality in exhausted CAR-T cells through epigenetic remodeling. Science *372*, eaba1786. https://doi.org/10.1126/science.aba1786.

38. Lynn, R.C., Weber, E.W., Sotillo, E., Gennert, D., Xu, P., Good, Z., Anbunathan, H., Lattin, J., Jones, R., Tieu, V., et al. (2019). c-Jun overexpression in CAR T cells induces exhaustion resistance. Nature *576*, 293–300. https://doi.org/10.1038/s41586-019-1805-z.

39. Giordano, M., Roncagalli, R., Bourdely, P., Chasson, L., Buferne, M., Yamasaki, S., Beyaert, R., Van Loo, G., Auphan-Anezin, N., Schmitt-Verhulst, A.M., and Verdeil, G. (2014). The tumor necrosis factor alpha-induced protein 3 (TNFAIP3, A20) imposes a brake on antitumor activity of CD8 T cells. Proc. Natl. Acad. Sci. USA *111*, 11115–11120. https://doi.org/10.1073/pnas.1406259111.

40. Banerjee, D., Liou, H.C., and Sen, R. (2005). C-Rel-dependent priming of naive T cells by inflammatory cytokines. Immunity *23*, 445–458. https://doi.org/10.1016/j.immuni.2005.09.012.

41. Balasubramani, A., Shibata, Y., Crawford, G.E., Baldwin, A.S., Hatton, R.D., and Weaver, C.T. (2010). Modular utilization of distal cis-regulatory elements controls Ifng gene expression in T cells activated by distinct stimuli. Immunity *33*, 35–47. https://doi.org/10.1016/j.immuni.2010.07.004.

42. Sica, A., Dorman, L., Viggiano, V., Cippitelli, M., Ghosh, P., Rice, N., and Young, H.A. (1997). Interaction of NF-kappaB and NFAT with the interferon-gamma promoter. J. Biol. Chem. *272*, 30412–30420. https://doi.org/10.1074/jbc.272.48.30412.

43. Grumont, R., Lock, P., Mollinari, M., Shannon, F.M., Moore, A., and Gerondakis, S. (2004). The mitogen-induced increase in T cell size involves PKC and NFAT activation of Rel/NF-kappaB-dependent c-myc expression. Immunity *21*, 19–30. https://doi.org/10.1016/j.immuni.2004.06.004.

44. Venkataraman, L., Burakoff, S.J., and Sen, R. (1995). FK506 inhibits antigen receptor-mediated induction of c-rel in B and T lymphoid cells. J. Exp. Med. *181*, 1091–1099. https://doi.org/10.1084/jem.181.3.1091.

45. Johnson, B.V., Bert, A.G., Ryan, G.R., Condina, A., and Cockerill, P.N. (2004). Granulocyte-Macrophage Colony-Stimulating Factor Enhancer Activation Requires Cooperation between NFAT and AP-1 Elements and Is Associated with Extensive Nucleosome Reorganization. Mol. Cell Biol. *24*, 7914–7930. https://doi.org/10.1128/mcb.24.18.7914-7930.2004.

46. Macián, F., López-Rodríguez, C., and Rao, A. (2001). Partners in transcription: NFAT and AP-1. Oncogene *20*, 2476–2489. https://doi.org/10.1038/sj.onc.1204386.

47. Chappert, P., and Schwartz, R.H. (2010). Induction of T cell anergy: Integration of environmental cues and infectious tolerance. Curr. Opin. Immunol. *22*, 552–559. https://doi.org/10.1016/j.coi.2010.08.005.

48. Harberts, A., Schmidt, C., Schmid, J., Reimers, D., Koch-Nolte, F., Mittrücker, H.W., and Raczkowski, F. (2021). Interferon regulatory factor 4 controls effector functions of CD8+ memory T cells. Proc. Natl. Acad. Sci. USA *118*, e2014553118. https://doi.org/10.1073/pnas.2014553118.

49. Gray, S.M., Amezquita, R.A., Guan, T., Kleinstein, S.H., and Kaech, S.M. (2017). Polycomb Repressive Complex 2-Mediated Chromatin Repression Guides Effector CD8+ T Cell Terminal Differentiation and Loss of Multipotency. Immunity *46*, 596–608. https://doi.org/10.1016/j.immuni.2017.03.012.

50. Seo, H., González-Avalos, E., Zhang, W., Ramchandani, P., Yang, C., Lio, C.W.J., Rao, A., and Hogan, P.G. (2021). BATF and IRF4 cooperate to counter exhaustion in tumor-infiltrating CAR T cells. Nat. Immunol. *22*, 983–995. https://doi.org/10.1038/s41590-021-00964-8.

51. Glasmacher, E., Agrawal, S., Chang, A.B., Murphy, T.L., Zeng, W., Vander Lugt, B., Khan, A.A., Ciofani, M., Spooner, C., Rutz, S., et al. (2012). A genomic regulatory element that directs assembly and function of immune-specific AP-1-IRF compelxes. Science (1979) *338*, 975–980.

52. Li, P., Spolski, R., Liao, W., Wang, L., Murphy, T.L., Murphy, K.M., and Leonard, W.J. (2012). BATF-JUN is critical for IRF4-mediated transcription in T cells. Nature *490*, 543–546. https://doi.org/10.1038/nature11530.

53. Iwata, A., Durai, V., Tussiwand, R., Briseño, C.G., Wu, X., Grajales-Reyes, G.E., Egawa, T., Murphy, T.L., and Murphy, K.M. (2017). Quality of TCR signaling determined by differential affinities of enhancers for the composite BATF-IRF4 transcription factor complex. Nat. Immunol. *18*, 563–572. https://doi.org/10.1038/ni.3714.

54. Wang, X., He, Q., Shen, H., Xia, A., Tian, W., Yu, W., and Sun, B. (2019). TOX promotes the exhaustion of antitumor CD8+ T cells by preventing

PD1 degradation in hepatocellular carcinoma. J. Hepatol. *71*, 731–741. https://doi.org/10.1016/j.jhep.2019.05.015.

55. Lee, C.G., Kang, K.H., So, J.S., Kwon, H.K., Son, J.S., Song, M.K., Sahoo, A., Yi, H.J., Hwang, K.C., Matsuyama, T., et al. (2009). A distal cis-regulatory element, CNS-9, controls NFAT1 and IRF4-mediated IL-10 gene activation in T helper cells. Mol. Immunol. *46*, 613–621. https://doi.org/10.1016/j.molimm.2008.07.037.

56. Rengarajan, J., Mowen, K.A., McBride, K.D., Smith, E.D., Singh, H., and Glimcher, L.H. (2002). Interferon regulatory factor 4 (IRF4) interacts with NFATc2 to modulate interleukin 4 gene expression. J. Exp. Med. *195*, 1003–1012. https://doi.org/10.1084/jem.20011128.

57. Martinez, G.J., Pereira, R.M., Äijö, T., Kim, E.Y., Marangoni, F., Pipkin, M.E., Togher, S., Heissmeyer, V., Zhang, Y.C., Crotty, S., et al. (2015). The transcription factor NFAT promotes exhaustion of activated CD8+ T cells. Immunity *42*, 265–278. https://doi.org/10.1016/j.immuni.2015.01.006.

58. Oestreich, K.J., Yoon, H., Ahmed, R., and Boss, J.M. (2008). NFATc1 Regulates PD-1 Expression upon T Cell Activation. J. Immunol. *181*, 4832–4839. https://doi.org/10.4049/jimmunol.181.7.4832.

59. Frebel, H., Nindl, V., Schuepbach, R.A., Braunschweiler, T., Richter, K., Vogel, J., Wagner, C.A., Loffing-Cueni, D., Kurrer, M., Ludewig, B., and Oxenius, A. (2012). Programmed death 1 protects from fatal circulatory failure during systemic virus infection of mice. J. Exp. Med. *209*, 2485–2499. https://doi.org/10.1084/jem.20121015.

60. Barber, D.L., Wherry, E.J., Masopust, D., Zhu, B., Allison, J.P., Sharpe, A.H., Freeman, G.J., and Ahmed, R. (2006). Restoring function in exhausted CD8 T cells during chronic viral infection. Nature *439*, 682–687. https://doi.org/10.1038/nature04444.

61. Mueller, S.N., Vanguri, V.K., Ha, S.J., West, E.E., Keir, M.E., Glickman, J.N., Sharpe, A.H., and Ahmed, R. (2010). PD-L1 has distinct functions in hematopoietic and nonhematopoietic cells in regulating T cell responses during chronic infection in mice. J. Clin. Invest. *120*, 2508–2515. https://doi.org/10.1172/JCI40040.

62. Lim, W.A., and June, C.H. (2017). The Principles of Engineering Immune Cells to Treat Cancer. Cell *168*, 724–740. https://doi.org/10.1016/j.cell.2017.01.016.

63. Lehmann, F., Marchand, M., Hainaut, P., Pouillart, P., Sastre, X., Ikeda, H., Boon, T., and Coulie, P.G. (1995). Differences in the antigens recognized by cytolytic T cells on two successive metastases of a melanoma patient are consistent with immune selection. Eur. J. Immunol. *25*, 340–347.

64. Van Den Eynde, B., Hainaut, P., Hérin, M., Knuth, A., Lemoine, C., Weynants, P., Van Der Bruggen, P., Fauchet, R., and Boon, T. (1989). Presence on a human melanoma of multiple antigens recognized by autologous CTL. Int. J. Cancer *44*, 634–640.

65. Stewart, S.A., Dykxhoorn, D.M., Palliser, D., Mizuno, H., Yu, E.Y., An, D.S., Sabatini, D.M., Chen, I.S.Y., Hahn, W.C., Sharp, P.A., et al. (2003). Lentivirus-delivered stable gene silencing by RNAi in primary cells. RNA *9*, 493–501. https://doi.org/10.1261/rna.2192803.

66. Barger, C.J., Branick, C., Chee, L., and Karpf, A.R. (2019). Pan-cancer analyses reveal genomic features of FOXM1 overexpression in cancer. Cancers *11*, 251. https://doi.org/10.3390/cancers11020251.

67. Krönke, J., Udeshi, N.D., Narla, A., Grauman, P., Hurst, S.N., McConkey, M., Svinkina, T., Heckl, D., Comer, E., Li, X., et al. (2014). Lenalidomide causes selective degradation of IKZF1 and IKZF3 in multiple myeloma cells. Science *343*, 301–305. https://doi.org/10.1126/science.1244851.

68. Seki, A., and Rutz, S. (2018). Optimized RNP transfection for highly efficient CRISPR/Cas9-mediated gene knockout in primary T cells. J. Exp. Med. *215*, 985–997. https://doi.org/10.1084/jem.20171626.

69. Roederer, M. (2011). Interpretation of cellular proliferation data: Avoid the panglossian. Cytometry A. *79*, 95–101. https://doi.org/10.1002/cyto.a.21010.

70. George, T.C., Fanning, S.L., Fitzgerald-Bocarsly, P., Medeiros, R.B., Highfill, S., Shimizu, Y., Hall, B.E., Frost, K., Basiji, D., Ortyn, W.E., et al. (2006). Quantitative measurement of nuclear translocation events using similarity analysis of multispectral cellular images obtained in flow. J. Immunol. Methods *311*, 117–129. https://doi.org/10.1016/j.jim.2006.01.018.

71. Maguire, O., O'Loughlin, K., and Minderman, H. (2015). Simultaneous assessment of NF-κB/p65 phosphorylation and nuclear localization using imaging flow cytometry. J. Immunol. Methods *423*, 3–11. https://doi.org/10.1016/j.jim.2015.03.018.

72. Picelli, S., Faridani, O.R., Björklund, A.K., Winberg, G., Sagasser, S., and Sandberg, R. (2014). Full-length RNA-seq from single cells using Smart-seq2. Nat. Protoc. *9*, 171–181. https://doi.org/10.1038/nprot.2014.006.

73. Liberzon, A., Birger, C., Thorvaldsdóttir, H., Ghandi, M., Mesirov, J.P., and Tamayo, P. (2015). The Molecular Signatures Database (MSigDB) hallmark gene set collection. Cell Syst. *1*, 417–425. https://doi.org/10.1016/j.cels.2015.12.004.

74. Doering, T.A., Crawford, A., Angelosanto, J.M., Paley, M.A., Ziegler, C.G., and Wherry, E.J. (2012). Network Analysis Reveals Centrally Connected Genes and Pathways Involved in CD8+ T Cell Exhaustion versus Memory. Immunity *37*, 1130–1144. https://doi.org/10.1016/j.immuni.2012.08.021.

STAR★METHODS

KEY RESOURCES TABLE

REAGENT or RESOURCE	SOURCE	IDENTIFIER
Antibodies		
Mouse APC/Cyanine7 anti-human CD19	BioLegend	Cat# 363010; RRID:AB_2564193
Mouse APC/Cyanine7 anti-human CD20	BioLegend	Cat# 302314; RRID:AB_314262
Mouse APC/Cyanine7 anti-human CD33	BioLegend	Cat# 366613; RRID:AB_2566415
Mouse APC/Cyanine7 anti-human CD326	BioLegend	Cat# 324245; RRID:AB_2783193
Mouse BV480 anti-human CD2	BD Biosciences	Cat# 746538; RRID:AB_2743830
Mouse PerCP Cy5.5 anti-human CD8β	BD Biosciences	N/A (custom order, 2ST8.5H7 clone as the CD8β BV421 and APC antibodies below)
Mouse BV421 anti-human CD8β	BD Biosciences	Cat# 742390; RRID:AB_2740746
Mouse APC anti-human CD8β	BD Biosciences	Cat# 641058; RRID:AB_1645723
Mouse BV650 anti-human CD197 (CCR7)	BioLegend	Cat# 353233; RRID:AB_2562041
Mouse PE anti-human CD197 (CCR7)	Biolegend	Cat# 353204; RRID:AB_10913813
Mouse FITC anti-human CD45RA	Biolegend	Cat# 304148; RRID:AB_2564157
Mouse Alexa 700 anti-human CD45RA	Biolegend	Cat# 304119; RRID:AB_493762
Mouse BV785 anti-human CD279 (PD-1)	Biolegend	Cat# 329930; RRID:AB_2563443
Mouse PE/Cyanine7 anti-human CD279 (PD-1)	Biolegend	Cat# 329918; RRID:AB_2159324
Mouse PE/Cyanine7 anti-human CD223 (LAG-3)	Biolegend	Cat# 369310; RRID:AB_2629753
Mouse BV421 anti-human CD137 (4-1BB)	Biolegend	Cat# 309819; RRID:AB_10895902
Mouse PE anti-human CD137 (4-1BB)	Biolegend	Cat# 309803; RRID:AB_314782)
Mouse BV650 anti-human CD69	Biolegend	Cat# 310934; RRID:AB_2563158
Mouse BV480 anti-human CD38	BD Biosciences	Cat# 566137; RRID:AB_2739535
Mouse FITC anti-human CD107a (LAMP-1)	BD Biosciences	Cat# 555800; RRID:AB_396134
Recombinant APC anti-human/mouse TOX	Miltenyi Biotec	Cat# 130-11-335; RRID:AB_2751485
Rat PE/Cyanine7 anti-human/mouse IRF4	BioLegend	Cat# 646414; RRID:AB_2728480
Rat Alexa 647 anti-human/mouse IRF4	BioLegend	Cat# 646408; RRID:AB_2564048
Rabbit Alexa 488 anti-human/mouse BATF	Cell Signaling Technology	Cat# 8638; RRID:AB_11141425
Rabbit PE anti-human/mouse BATF	Cell Signaling Technology	Cat# 8638; RRID:AB_11141425
Mouse Alexa 488 anti-human Ki-67	BD Biosciences	Cat# 558616; RRID:AB_647087
Mouse BV421 anti-human Ki-67	BD Biosciences	Cat# 562899; RRID:AB_2686897
Mouse Alexa 700 anti-human IFNγ	BioLegend	Cat# 502520; RRID:AB_528921
Mouse BV421 anti-human TNFα	BioLegend	Cat# 502931; RRID:AB_10898321
Mouse Alexa 700 anti-human TNFα	BioLegend	Cat# 502927; RRID:AB_2561314
Rat APC anti-human GM-CSF	BioLegend	Cat# 502310; RRID:AB_11150231
Mouse Alexa 488 anti-human Histone H1	Santa-Cruz Biotechnology	Cat# sc-8030; RRID:AB_675641
Mouse Alexa 647 anti-human Histone H1	Santa-Cruz Biotechnology	Cat# sc-8030; RRID:AB_675641
Rabbit Alexa 647 anti-human NF-κB (p65)	Cell Signaling Technology	Cat# 8801; RRID:AB_2797670
PE/Cyanine 7 Rat IgG1, k isotype ctrl	BioLegend	Cat# 400416; RRID:AB_326522
Alexa Fluor 647 Rat IgG1, k isotype ctrl	BioLegend	Cat# 400418; RRID:AB_389341
Rabbit (DA1E) mAb IgG XP Isotytpe Control (PE Conjugate)	Cell Signaling Technology	Cat# 5742; RRID:AB_10694219
Rabbit (DA1E) mAb IgG XP Isotytpe Control (Alexa 488 Conjugate)	Cell Signaling Technology	Cat# 2975; RRID:AB_10699151
Brilliant Violet 421 Mouse IgG1, k isotype ctrl	BioLegend	Cat# 400158; RRID:AB_11150232
Purified NA/LE Mouse anti-human CD28	BD Biosciences	Cat# 555725; RRID:AB_396068
Ultra-LEAF Purified anti-human CD3	BioLegend	Cat# 317352; RRID:AB_11150592
FcR Blocking Reagent, human	Miltenyi Biotec	Cat# 130-059-901; RRID:AB_2892112
CD8 MicroBeads, human	Miltenyi Biotec	Cat# 130-045-201; RRID:AB_2889920

(Continued on next page)

Continued

REAGENT or RESOURCE	SOURCE	IDENTIFIER
Bacterial and virus strains		
2ND generation lentiviral particles (RFP/IRF4 ind)	Home-made	N/A
2ND generation lentiviral particles (RFP/IRF4 ind)	VectorBuilder	Custom Order
CD5L-OKT3scFv-CD14 lentiviral particles of 2ND generation	Home-made	N/A
Biological samples		
Hemochromatosis blood samples	Clinique Saint-Luc	N/A
COVID-19 blood samples	Clinique Saint-Luc	N/A
Ovarian cancer tumor and blood samples	Clinique Saint-Luc	N/A
Chemicals, peptides, and recombinant proteins		
Fixable Viability Dye eFluor 780	eBioscience	Cat# 65-0865-14
Iscove's Modified Dulbecco's Medium (IMDM)	ThermoFisher	Cat# 21980065
Dulbecco's Modified Eagle Medium (DMEM)	ThermoFisher	Cat# 31885023
GlutaMAX Supplement	ThermoFisher	Cat# 350500038
Fetal Bovine Serum (FBS)	Sigma-Aldrich	Cat# F7524
2-Mercaptoethanol	Sigma-Aldrich	Cat# M3148
Penicillin-Streptomycin	Sigma-Aldrich	Cat# P4333
Dynabeads Human T-Activator CD3/CD28	ThermoFisher	Cat# 11132D
LymphoPrep^{TM}	Serumwerk	Cat# 1858-1
EDTA	ThermoFisher	Cat# 15575-038
Liberase DL Research Grade	Sigma-Aldrich	Cat# 5466202001
Liberase TL Research Grade	Sigma-Aldrich	Cat# 5401020001
Deoxyribonuclease I (DNase I)	Worthington	Cat# LS002060
IL-2 (aldesleukine (Proleukine))	Novartis	Cat# CNK 1185-958
Dimethyl sulfoxide (DMSO)	Santa Cruz Biotechnology	Cat# sc-358801
Gentamicin solution	Sigma-Aldrich	Cat# G1397
Lenti-X Concentrator	Takara	Cat# 631232
Trypan blue	Sigma-Aldrich	Cat# T8154
Türk's solution	Merck	Cat# 109277
Opti-MEM I Reduced Serum Medium	ThermoFisher	Cat# 11058021
Doxycycline hyclate	Sigma-Aldrich	Cat# D9891
DEPC-treated water	ThermoFisher	Cat# AM9906
TrueCut Cas9 Protein v2	ThermoFisher	Cat# A36499
Brefeldin A	Sigma-Aldrich	Cat# B7651
Phorbol 12-Myristate 13-Acetate (PMA)	LC Laboratories	Cat# P-1680
Ionomycin calcium salt	Sigma-Aldrich	Cat# I0634
IKK16	MedChemExpress	Cat# HY-13687
FK506	MedChemExpress	Cat #HY-13756
Hoechst 33342 Solution	ThermoFisher	Cat# 62249
RNasin Plus Ribonuclease Inhibitor	Promega	Cat# N2615
Sodium Acetate (3M), pH 5.5, RNase-free	ThermoFisher	Cat# AM9740
Glycogen, RNA grade	ThermoFisher	Cat# R0551
Ethanol absolute >99,8%, AnalaR NORMAPUR	VWR	Cat# 20821.296P
SuperScript II Reverse Transcriptase	ThermoFisher	Cat# 18064071
KAPA HiFi HotStart DNA Polymerase	Roche	Cat# 07958897001
AMPure XP Paramagnetic beads	Beckman Coulter	Cat# A63881
CaCl2	Home-made	N/A
HeBS	Home-made	N/A

(Continued on next page)

Continued

REAGENT or RESOURCE	SOURCE	IDENTIFIER
Critical commercial assays		
RecoverAll Total Nucleic Acid Isolation Kit FFPE	ThermoFisher	Cat# AM1975
P3 Primary Cell 4D-Nucleofector	Lonza	Cat# V4XP-3024
CellTrace Violet Cell Proliferation Kit	ThermoFisher	Cat# C34557
eBioscience Foxp3/transcription factor staining buffer set	ThermoFisher	Cat# 00-5523-00
QuantiFluor dsDNA System	Promega	Cat# E2670
Nextera XT DNA Library Preparation Kit	Illumina	Cat# FC-131-1096
Nextera XT Index Kit v2 Set D	Illumina	Cat# FC-131-2004
DNA ScreenTape Analysis	Agilent	Cat# 5067-5588
DNA ScreenTape Analysis	Agilent	Cat# 5067-5589
Takyon™ ROX Probe 2× MasterMix dTTP	Eurogentec	Cat #UF-RPMT-B0701
Deposited data		
RNAseq data of IRF4^{dox}, RFP^{dox}, ctrl, IRF4^{KO}	Gene expression Omnibus	Database GEO: GSE245739
Results of GSEA on Hallmark gene collections and on Exhaustion gene signatures (Table S1)	N/A	N/A
List of leading-edges genes for GSEA (Table S2)	N/A	N/A
Experimental models: Cell lines		
LB33-MELA.1	Lehmann et al.[63]	De Duve Institute
MZ2-MEL.43	Van Den Eynde et al.[64]	De Duve Institute
HEK293T/17	ATCC	CRL-11268
Oligonucleotides		
TrueGuide sgRNA Negative Control	ThermoFisher	Cat# A35526
TrueGuide synthetic sgRNA CRISPR 998515_SGM	ThermoFisher	Cat# A35533
TrueGuide synthetic sgRNA CRISPR 998503_SGM	ThermoFisher	Cat# A35533
RT-qPCR and RNAseq library primers	Eurogentec	N/A
Recombinant DNA		
CD5L-OKT3scFv-CD14 gBlocks gene fragment	IDTdna	Custom Order; sequence in Table S3
pCMV-VSV-G	Stewart et al.[65]	RRID:Addgene_8454
psPAX2	Didier Trono lab	RRID:Addgene_12260
pCW57-MCS1-P2A-MCS2 (RFP)	Barger et al.[66]	RRID:Addgene_80923
Plenti-CAG-IRF4-FLAG-IRES-GFP	Krönke et al.[67]	RRID:Addgene_107389
pTM941-hPGK-TOX	Home-made	N/A
pLV-TRE3G>MCS-hPGK>EGFP:T2A:Tet3G	VectorBuilder	Custom Order
Software and algorithms		
Qlucore Omics Explorer	Qlucore, Lund	https://qlucore.com/
FlowJo 10.9.0	FlowJo	https://www.flowjo.com/
IDEAS ImageStream	Cytek Bioscience	https://cytekbio.com/pages/imagestream
Prism 8.0	GraphPad	https://www.graphpad.com/features
DSEeq2	Bioconductor	https://bioconductor.org/packages/release/bioc/html/DESeq2.html
Other		
High-binding 96-well flat-bottom plates	Greiner	Cat# 655061

RESOURCE AVAILABILITY

Lead contact

Further information and requests for resources and reagents should be directed to and will be fulfilled by the lead contact, Thibault Hirsch (thibault.hirsch@uclouvain.be).

Materials availability

This study generated new plasmids, which would be available from the lead contact upon request and, if necessary, the signing of a Material Transfer Agreement.

Data and code availability

- The RNAseq data are available at Gene Expression Omnibus database under accession number GSE245739.
- This paper does not report original code.
- Any additional information required to reanalyze the data reported in this paper is available from the lead contact upon request.

EXPERIMENTAL MODEL AND STUDY PARTICIPANT DETAILS

Table 1 below: Hemochromatosis non-cancerous donors whose blood was used in this study.

Donor	Age	Gender	Purpose
LB-3149	63	M	Generate IRF4^{dox} or IRF4^{ko} CD8 T-cells
LB-9847	28	M	Generate IRF4^{dox} or IRF4^{ko} CD8 T-cells
LB-6019	43	M	Generate IRF4^{dox} or IRF4^{ko} CD8 T-cells
LB-5660	54	M	Generate IRF4^{dox} or IRF4^{ko} CD8 T-cells
LB-9481	69	M	Generate IRF4^{dox} or IRF4^{ko} CD8 T-cells
LB-3419	53	na	Generate IRF4^{dox} or IRF4^{ko} CD8 T-cells
LB-3318	49	M	Generate IRF4^{dox} or IRF4^{ko} CD8 T-cells
LB-9928	63	F	Generate IRF4^{dox} or IRF4^{ko} CD8 T-cells
LB-833	54	M	Generate IRF4^{dox} or IRF4^{ko} CD8 T-cells
LB-9862	52	F	Generate IRF4^{dox} or IRF4^{ko} CD8 T-cells
LB-1117	66	M	Generate IRF4^{dox} or IRF4^{ko} CD8 T-cells
LB-3329	58	M	Generate IRF4^{dox} or IRF4^{ko} CD8 T-cells
LB-9853	69	M	Generate IRF4^{dox} or IRF4^{ko} CD8 T-cells
LB-9335	59	M	Generate IRF4^{dox} or IRF4^{ko} CD8 T-cells
LB-3305	64	M	Generate IRF4^{dox} or IRF4^{ko} CD8 T-cells
LB-9288	61	M	Generate IRF4^{dox} or IRF4^{ko} CD8 T-cells
LB-6002	73	F	Generate IRF4^{dox} or IRF4^{ko} CD8 T-cells
LB-9898	45	M	Generate IRF4^{dox} or IRF4^{ko} CD8 T-cells
LB2960	49	M	Generate IRF4^{dox} or IRF4^{ko} CD8 T-cells
LB6000	58	M	Generate IRF4^{dox} or IRF4^{ko} CD8 T-cells
LB9991	60	M	Generate IRF4^{dox} or IRF4^{ko} CD8 T-cells
LB3380	F	69	Generate IRF4^{dox} or IRF4^{ko} CD8 T-cells
LB5992	M	50	Generate IRF4^{dox} or IRF4^{ko} CD8 T-cells
LB-9443	61	M	Compare with COVID-19 or ovarian cancer samples
LB-569	74	M	Compare with COVID-19 or ovarian cancer samples
LB-5949	67	M	Compare with COVID-19 or ovarian cancer samples
LB-6022	44	M	Compare with COVID-19 or ovarian cancer samples
LB-3329	58	M	Compare with COVID-19 or ovarian cancer samples
LB-9335	59	M	Compare with COVID-19 or ovarian cancer samples

Table 2 below: Patients with ovarian cancer whose blood or tumor were used in this study.

Patient	Age	Pathology	FIGO	Neoadjuvant chemotherapy
LB-6151	75	Endometrioid carcinoma	IIA	No
LB-9189	35	Grade 3 serous carcinoma	IIIC	No

(Continued on next page)

Continued

Patient	Age	Pathology	FIGO	Neoadjuvant chemotherapy
LB-9280	70	Grade 3 serous carcinoma	IIIC	No
LB-9256	72	Grade 3 serous carcinoma	IIIC	No
LB-9227	58	Grade 3 serous carcinoma	IIIC	No
LB-9168	54	Grade 3 serous carcinoma	IIIC	No
LB-9269	63	Grade 3 serous carcinoma	IIIA2	No
LB-9207	83	Low grade serous carcinoma	IIIC	No
LB-9238	60	Grade 3 serous carcinoma	IIIC	No
LB-9148	56	Grade 3 serous carcinoma	IVB	No
LB-9202	72	Grade 3 serous carcinoma	IIIC	Yes
LB-9240	55	Grade 3 serous carcinoma	IVB	Yes
LB-9257	49	Grade 3 serous carcinoma	IIIC	no

Table 3 below: Patients with COVID-19 whose blood was used in this study. Non-ICU = sample retrieved from patient not hospitalized in intensive care unit. Pre-ICU = sample retrieved from patient before hospitalization in intensive care unit. ICU = sample retrieved from patient hospitalized in intensive care unit.

Patient	Age	Gender	Sample	Hospitalisation stage
LB-9379	67	M	1	Non-ICU
LB-9333	39	M	1	Non-ICU
LB-9358	61	na	1	Non-ICU
LB-9405	68	M	1	ICU
LB-9367	59	M	1	ICU
LB-9313	59	M	1	ICU
LB-9310	62	M	1	Pre-ICU
LB-9387	68	M	1	ICU
LB-9381	73	M	1	Non-ICU
LB-9322	51	M	1	Non-ICU
LB-9325	50	M	1	Non-ICU
LB-9395	63	M	1	Pre-ICU
LB-9395	63	M	2	ICU
LB-9309	27	M	1	Non-ICU
LB-9309	27	M	2	Non-ICU
LB-9319	74	F	1	Non-ICU
LB-9319	74	F	2	Non-ICU
LB-9342	50	na	1	Pre-ICU
LB-9342	50	na	1	Pre-ICU
LB-9342	50	na	2	ICU

METHOD DETAILS

Cell culture and media

Tumor line LB33-MEL.A.1[63] was cultured in Iscove's Modified Dulbecco's Medium (IMDM) (ThermoFisher, #21980065) supplemented with 10% fetal bovine serum (FBS) (Sigma-Aldrich, #F7524), 1.5mM GlutaMAX (ThermoFisher, #350500038), 50μM 2-mercaptoethanol (Sigma-Aldrich, #M3148), 100U/mL penicillin and 100 μg/mL streptomycin (Sigma-Aldrich, #P4333). Cells were maintained at 37°C, 8% CO_2. Tumor line MZ2-MEL.43[64] was cultured in Dulbecco's Modified Eagle Medium (DMEM) (ThermoFisher, #31885023) supplemented with 10% FBS, 1.5mM GlutaMAX, 100U/mL penicillin and 100 μg/mL streptomycin. Cells were maintained at 37°C, 8% CO_2. The HEK293T line was cultured in DMEM medium supplemented with 10% FBS, 1.5mM GlutaMAX, 1μM sodium pyruvate (J.T Baker), 100U/mL penicillin and 100 μg/mL streptomycin. CD8 T cells isolated from blood of

donors with hemochromatosis were amplified with anti-CD3/CD28 beads (ThermoFisher, #11132D) at a ratio of 1 bead per 3 cells in IMDM medium supplemented with 10% human serum (HS) (Ludwig Institute for Cancer Research (LICR), Brussels Branch), 1.5mM GlutaMAX, 100U/mL penicillin, 100 μg/mL streptomycin, and 500IU/mL of interleukin-2 (IL-2) (Proleukine, Novartis, #CNK 1185-958). Cells were maintained at 37°C, 8% CO_2. Whenever necessary, T cells were divided in 2 and IL-2 refreshed in the medium.

Tumor and peripheral blood mononuclear cells isolation from patients

The samples were obtained from the Cliniques Universitaires Saint-Luc (CUSL) with approval of the CUSL ethical committee (2017/11OCT/478 – Belgian n°: B403201734113, 2020/27AVR/246 and 2022/14NOV/423 – Belgian n°: BE4032022000129), and was carried out in accordance with the principles expressed in the Declaration of Helsinki. Patients gave written informed consent, and their records were anonymized prior to the analysis. The cohorts of patients are described in Tables 2 and 3. Peripheral blood mononuclear cells (PBMCs) from patients with COVID-19 or ovarian carcinoma were isolated by density gradient. Blood was layered over a solution of Lymphoprep (Serumwerk, #1858) and centrifuged at 870g for 20 min with minimal acceleration and deceleration. The ring of mononuclear cells was recovered and washed 3 times with PBS + 1mM EDTA (ThermoFisher, #15575-038) to remove platelets. The 1st centrifugation was performed at 400g for 10 min, and the following two at 300g for 7 min. Ovarian tumor samples were cut into small pieces and transferred to PBS containing the enzymes liberase low dispase (Sigma-Aldrich, #5466202001) and liberase low thermolysin (Sigma-Aldrich, #5401020001) at the recommended concentrations, plus 10 Kunitz/mL DNase I (Worthington, #LS002060). A first mechanical dissociation with MACS dissociator (Miltenyi) was performed, then samples were incubated for 45 min at 37°C. A second mechanical dissociation with MACS dissociator was performed, then cells were washed with PBS EDTA 1mM before being centrifuged for 10 min at 400g. Cells were resuspended in PBS EDTA 1mM, filtered through 40μM mesh, and washed with PBS EDTA 1mM. Cells were then layered on a solution of Lymphoprep and processed as described above. Once obtained, PBMCs and tumor mononuclear cells suspensions were counted with Türk's solution (Merck, #109277) and trypan blue (Sigma-Aldrich, #T8154), respectively, using a hematimeter. Cells were centrifuged for 7 min at 300g and resuspended in 50% IMDM, 40% HS and 10% DMSO (Santa Cruz Biotechnology, #sc-358801 for freezing at −80°C. Frozen cells were then stored at −180°C in liquid nitrogen.

CD8 T-cell isolation from non-cancerous donors

PBMCs from non-cancerous control individuals were obtained from blood of hemochromatosis patients by density gradient as described above. The cohort of patients is described in Table 1. The PBMCs obtained were resuspended at 2.10^8/mL in PBS EDTA 1mM HS 1% containing 20% FcR block (Miltenyi, #130-059-901) and 20% CD8 microbeads (Miltenyi, 130-045-201) for 15 min at 4°C. Cells were filtered through 40μM mesh, volume adjusted to 0.5mL, and cells sorted by AutoMACS (Miltenyi) in possel_s mode in PBS EDTA 1mM HS 1% Gentamicin 15 μg/mL (Sigma-Aldrich, #G1397). The positive fraction containing CD8 T cells was counted with trypan blue. Cells were washed with IMDM and frozen in 50% IMDM, 40% HS and 10% DMSO.

Plasmids and lentiviral production

For lentiviral particle production, the plasmids pCMV-VSV-G (Addgene, #8454) and psPAX2 (Addgene, #12260) were used with the transfer plasmid pLV-TRE3G>MCS-hPGK>EGFP:T2A:Tet3G (VectorBuilder, custom order) encoding RFP or IRF4 or TOX. The RFP-encoding sequence was cloned from the plasmid pCW57-MCS1-P2A-MCS2 (Addgene, #80923), the IRF4-encoding sequence was cloned from the plasmid plenti-CAG-IRF4-FLAG-IRES-GFP (Addgene, #107389), and the TOX-encoding sequence was cloned using the cDNA from activated human PBMCs. These sequences were then ligated into the multiple cloning site (MCS) of the transfer plasmid. For all experiments except the ones for analysis of NF-κB translocation, lentiviral particles were produced as follow. The day before transfection, 10^7 HEK293T were plated in $175cm^2$ flasks in 20mL antibiotic-free complete medium. For each flask, the following mixture was made: 15μg pCMV-VSV-G plasmid, 30μg psPAX2 plasmid, and 45μg transfer plasmid (inducible IRF4 or RFP), 400μL calcium chloride ($CaCl2$) 2M, and water to adjust the volume to 2.5mL. To this mixture was added dropwise 2.5mL of HeBS. The 5mL plasmid-CaCl2-HeBS mixture was then transferred dropwise to HEK293T cells and incubated for 6h at 37°C 8% CO_2 before replenishing the flask with 20mL antibiotic-free complete medium. After 3 days at 37°C 8% CO_2, the supernatant containing viral particles was collected and centrifuged at 500g for 10 min at 4°C. The supernatant was harvested and deposited on 0.5 volume of Lenti-X Concentrator (Takara, #631232) before being incubated for 30 min at 4°C and then centrifuged at 1400g for 45 min at 4°C. The virus particle pellet was resuspended in Opti-MEM (ThermoFisher, #11058021) and frozen at −180°C. An aliquot of the virus particle solution was systematically used to estimate the concentration of effective virus particles obtained. For this purpose, the infection efficiency of the particles was estimated by incubating HEK293T cells for 48h with decreasing volumes of particles, then the proportion of infected cells for each condition was evaluated by flow cytometry.

For experiments to analyze the impact of IRF4 on NF-κB translocation, high number of cells was necessary, thus requiring to transduce many T cells at start. To have sufficient particles from a same batch, we outsourced lentiviral particles production to VectorBuilder Inc. that performed the operation using our inducible IRF4 and RFP transfer vectors. These lentiviral particles were used to transduce CD8 T cells for NF-κB translocation experiments.

CD8 T cell lentiviral transduction and doxycycline induction

CD8 T cells from donors with hemochromatosis were thawed, washed, and resuspended at 10^7/mL for 4h at 37°C 8% CO_2 in complete medium in the presence of 5 Kunitz/mL DNAse I. Cells were counted using trypan blue. In 96-well round-bottom plates (Corning,

#3799), 50,000 cells were plated, along with 500,000 lentiviral particles (1.10^6 particles for NF-κB experiments) and 16,666 anti-CD3/CD28 beads, in a final volume of 100 μL complete medium with IL-2 at 500UI/mL. The plate was then centrifuged for 2h at 400g and placed at 37°C 8% CO_2 for 4 days. Cells were then washed 3 times with complete medium, before being labeled in PBS EDTA 1mM HS 1% with anti-CD8β PerCP-Cy5.5 antibody (BD Biosciences, clone 2ST8.5H7) and viability probe eFluor780 (eBioscience, #65-0865-18) for 20 min at 4°C and then washed 2 times with PBS EDTA 1mM HS 1%. Live CD8β⁺ GFP⁺ T cells were sorted with FACS ARIA III (BD Biosciences) and amplified in complete medium in the presence of 500UI/mL IL-2. After 6 days, T cells were incubated for a further 48h with 1 μg/mL doxycycline (Sigma-Aldrich, #D9891) and 500UI/mL IL-2 before analyzing their effector functions, proliferation, activation markers expression, transcriptome, NF-κB translocation. Doxycycline was maintained at 1 μg/mL throughout the assays except in the experiments during which we activated T cell to induce NF-κB translocation since doxycycline emits fluorescence in the channel that was used to visualize cell nuclei.

CRISPR/Cas9

CD8 T cells from donors with hemochromatosis were thawed, washed, and resuspended at 10^7/mL for 4h at 37°C 8% CO_2 in complete medium in the presence of 5 Kunitz/mL DNAse I. Cells were counted with trypan blue and resuspended at 2.10^6 cells per 100μL in P3 electroporation buffer (Lonza, #V4XP-3024). Cas9-guide RNA complexes were prepared in RNAse free 1.5mL eppendorf tube by incubating for 5 min at RT°C in RNAse-free water (Ambion, #AM9906) 5μg of Cas9 (ThermoFisher, #A36499) with 150pmol of guide RNA control (ThermoFisher, #A35526) or 150pmol of guide RNA targeting *IRF4* exon 2 (ThermoFisher, #CRISPR 998515_SGM). This mixture was then added to the 2.10^6 cells to be nucleofected. After 2 min incubation at RT°C, the cell-Cas9-gRNA mixture was transferred into nucleocuvettes (Lonza, #V4XP-3024), and the cells were electroporated with the "T cell human unstim high-efficiency (FI115)" program from 4D Nucleofector (Lonza). Immediately after electroporation, 1mL of complete medium containing 500UI/mL IL-2 was added, and cells were transferred to 24-well plates to rest for 3h at 37°C 8% CO_2. After resting, 1mL of complete medium with 500UI/mL IL-2 and 666,666 anti-CD3/CD28 beads was added, and cells were incubated at 37°C 8% CO_2 for 5 days before analyzing their effector functions or transcriptome. Alternatively, cells that had recovered from electroporation were immediately used to initiate a proliferation assay and track activation markers expression.

For improved knock-out efficacy, we adapted an optimized version of CRISPR/Cas9 RNP transfection to our needs.[68] CD8 T cells from donors with hemochromatosis were thawed, washed, and resuspended at 2.10^6 cells/mL/cm² in a 24-well plate with 5 Kunitz/mL DNAse I. After overnight incubation at 37°C 8% CO_2, cells were counted with trypan blue, washed with 6 volumes of warm PBS, and resuspended at $1,5.10^6$ cells per 100μL in P3 electroporation buffer. Cas9-guide RNA complexes were prepared in RNAse-free 1.5mL ependorf by incubating for 10 min at room temperature 5 μg of Cas9 with 150pmol of guide RNA targeting *IRF4* exon 2 (ThermoFisher, #CRISPR 998515_SGM) + 150pmol of guide RNA targeting *IRF4* exon 2 (ThermoFisher, #CRISPR 998503_SGM), or with 300pmol of guide RNA control. In a round-bottom 96-well plate, $1,5.10^6$ cells in 100 μL P3 electroporation buffer were mixed with 5 μL of Cas9:gRNA mix. After 2 min incubation at RT°C, the cell-Cas9-gRNA mixture was transferred into nucleocuvettes, and the cells were electroporated with the "T cell human unstim high-efficiency (FI115)" program from 4D Nucleofector. Immediately after electroporation, 500 μL of pre-warmed complete medium containing 500UI/mL IL-2 was added, and cells were transferred to 48-well plates that had been preincubated for 20 min 37°C 8% CO2 with 500 μL complete medium + 500UI/mL IL-2. After 4h–6h of rest at 37°C 8% CO_2, cells were counted and activated as 40,000 T cells per well with 13,333 anti-CD3/CD28 beads, and incubated 2 days for *PDCD1* RT-qPCR experiments, 3 days for analysis of IRF4 knock-out efficacy and expression of activation markers by flow cytometry, and 5 days for cytokine gene expression analysis by RT-qPCR and flow cytometry.

Cytokine production assay

The day before the assay, 100 μL of PBS containing 1 μg/mL OKT3 anti-CD3ε antibody (Biolegend, #317326) were plated in high-binding 96-well flat-bottom plates (Greiner, #655061). The plate was incubated overnight at 4°C. On next day, PBS was removed and 100μL complete medium containing 500UI/mL IL-2 was immediately added. CD8 T cells at day 5 after CRISPR/Cas9 or at day 2 after doxycycline induction were counted with trypan blue and 100μL containing 75,000 T cells and 500UI/mL IL-2 were added. For stimulation with tumor lines LB33-MELA.1 and MZ2-MEL.43 OKT3-CD14, 75,000 T cells were cocultured with 75,000 tumor cells in round-bottom 96-well plates in 200μL with 500UI/mL IL-2. Activation was initiated after a brief centrifugation for 1 min at 400g and incubation at 37°C 8% CO_2. After 1h, Brefeldin A (BFA) (Sigma-Aldrich, #B7651) was added to each well at 5 μg/mL final concentration, and cells were incubated for a further 4h at 37°C 8% CO_2. Cells were then placed on ice and transferred to pre-cooled 96-well conical-bottom plates (Corning, #3894) before being washed and labeled for analysis by flow cytometry.

For tumor and blood PBMC samples from patients with ovarian carcinoma, cells were thawed at 10^7/mL for 4h at 37°C 8% CO_2 in complete medium supplemented with 5 Kunitz/mL DNAse I. Live cells were counted with trypan blue and resuspended in complete medium at 2.10^6/mL. PBS was removed from OKT3 wells and 100μL of complete medium containing or not a cocktail of phorbol 12-myristate 13-acetate (LC laboratories, #P-1680; final concentration 1 ng/mL) and ionomycin (Sigma-Aldrich, #I0634; final concentration 1 μg/mL) were immediately added. Then, 100μL containing 200,000 cells were added. For each condition, the cells were plated in 5 different wells that would then be pooled together for staining of 1.10^6 cells. Activation was initiated after a brief centrifugation for 1 min at 400g and incubation at 37°C 8% CO_2 for 5h in the presence of BFA, as explained above. The plate was placed on ice and cells from a same condition pooled together in pre-cooled 1.5mL eppendorf tubes. Cells were centrifuged for 5 min 400 g at 4°C, resuspended in

PBS EDTA 1mM HS 1% and transferred to pre-cooled 96-well conical-bottom plates before being labeled for analysis by flow cytometry.

Degranulation assay

CD8 T cells at day 5 after CRISPR/Cas9 were counted using trypan blue. In 96-well round-bottom plates, 75,000 T cells were cocultured with 75,000 tumor cells in 200μL with 500UI/mL IL-2 and 1.25 μg/mL anti-CD107a antibody (BD Biosciences, Clone H4A3). The plate was centrifuged for 1 min at 400g and then incubated for 1h at 37°C 8% CO_2. After 1h incubation, 5 μg/mL BFA was added to each well, and cells were incubated for a further 4h at 37°C 8% CO_2. Cells were then placed on ice and transferred to pre-cooled 96-well conical-bottom plates before being labeled for analysis by flow cytometry.

Proliferation assay and concomitant measurement of activation markers expression

The day before the proliferation assay, 100μL of PBS containing 1 μg/mL OKT3 anti-CD3ε antibody was plated in 96-well round-bottom plates. The plate was incubated overnight at 4°C. Frozen CD8 T cells on day 2 after induction with doxycycline were thawed in 1mL complete medium (up to 10^7/cells ml) with 5 Kunitz/mL DNAse I and live cells counted with trypan blue after 4h. Live CD8 T cells at 3h after CRISPR/Cas9 were counted with trypan blue, centrifuged, and loaded with 5μM CellTrace Violet (CTV) (ThermoFisher, #C34557) following manufacturer instructions. Cells were resuspended at 3.10^5/mL in complete medium with 500UI/mL IL-2. PBS containing OKT3 antibody was removed from the wells and 30,000 cells in 100 μl were added per well. When indicated, 2 μg/mL soluble anti-CD28 was added (BD Biosciences, #555725, Clone CD28.2). Cells were centrifuged for 1 min at 400g before being incubated for 3 to 4 days at 37°C 8% CO_2. On day 3 or 4 after activation, cells were placed on ice and transferred to pre-cooled 96-well conical-bottom plates before being labeled for flow cytometry analysis. The metrics used to assess T cell proliferation were calculated by the Flowjo proliferation platform.[69]

For assessment of PD-1 regulation by NF-κB or NFAT, CD8 T cells after CRISPR/Cas9 editing or at day 2 post doxycycline induction were activated for 3 days at 37°C 8% CO_2, as described. Activation occurred in the presence of absence of the NFAT inhibitor FK506 (MedChemExpress, #HY-13756) or the NF-κB inhibitor IKK16 (MedChemExpress, #HY-13687). While FK506 had little toxicity over 3 days of culture even at 3μM final concentration, IKK16 could not be used at more than 2-3μM for 3 days culture.

Extracellular and intracellular stainings for flow cytometry

Cells were harvested and transferred to pre-cooled 96-well conical-bottom plates. The plate was centrifuged at 400g for 4 min at 4°C. Cells were washed with 150μL PBS EDTA 1mM HS 1% and centrifuged for 4 min at 400g 4°C. Cells were resuspended in 50μL PBS EDTA 1mM HS 1% containing the appropriate antibodies. After 20 min, cells were washed 2× with 150μL PBS EDTA 1mM HS 1% and centrifuged for 4 min at 400g, 4°C. If intracellular staining was then performed, cells were washed one last time with 150μL PBS and centrifuged for 4 min at 400g, 4°C. Cells were then resuspended in 100μL fixation and permeabilization buffer (eBiosciences, #00-5523-00) before being incubated between 12h and 16 h at 4°C. Fixed and permeabilized cells were centrifuged for 5 min at 870g, 4°C. Cells were then washed 3× with 100μL permeabilization buffer (eBiosciences, #00-5523-00) and centrifuged for 5 min at 870g, 4°C. Cells were resuspended in 30μL blocking solution (permeabilization buffer + HS 8%) and incubated for 15 min at 4°C. Then, 20μL of permeabilization buffer containing the appropriate 2,5× concentrated antibodies was added. Cells were homogenized and incubated for 2h at 4°C. Cells were washed 3 times with 150μL permeabilization buffer and centrifuged for 5 min at 870g, 4°C. Cells were resuspended in permeabilization buffer and analyzed by flow cytometry using BD LSRII Fortessa (BD Biosciences). Data were analyzed on Flowjo (BD Biosciences). Proper cell fixation and permeabilization to reach nucleus was systematically controlled by histone H1 staining as depicted in Figure S1A.

For experiments in which we simultaneously compared the phenotype of CD8 T cells in ovarian carcinoma and COVID-19 samples, we thawed the cryotubes in water bath at 37°C, and immediately transferred the cell suspension in pre-cooled 15mL falcon tubes. 9mL cold PBS EDTA 1mM HS 1% was quickly added, and cells were centrifuged 7 min at 300g 4°C. All the rest of the procedure was done at 4°C. Transfer of cells to pre-cooled 96-well conical-bottom plates and extracellular staining were performed in presence of 5 Kunitz/mL DNase I. Fixation/permeabilization and subsequent steps were then performed as described above.

For experiment in which we simultaneously track the expression of activation markers over time after T cell stimulation, CD8 T cell were frozen at each timepoint and once all collected, thawed and processed in the same way as indicated right before.

NF-κB translocation assay

The day before the assay, 100 μl of PBS containing 1 μg/mL OKT3 anti-CD3ε antibody were plated in high-binding 96-well flat-bottom plates. The plate was incubated overnight at 4°C. On next day, PBS was removed and 100μL complete medium containing 500UI/mL IL-2 with or without the NF-κB inhibitor IKK16 (MedChemExpress, #HY-13687; final concentration 5μM) was immediately added. CD8 T cells at day 2 after doxycycline induction were counted with trypan blue and 100μL containing 200,000 T cells and 500UI/mL IL-2 were added. For each condition, the cells were plated in 4–5 different wells that would then be pooled together for staining of 8.10^5 to 1.10^6 cells. Activation was initiated after a brief centrifugation for 1 min at 400g and incubation at 37°C 8% CO_2. After each activation timepoint was reached, the plate was placed on ice and cells from a same condition immediately pooled together in pre-cooled 1.5mL eppendorf tubes. Cells were centrifuged for 5 min 400 g at 4°C, resuspended in 200μL PBS, and kept at 4°C in pre-cooled 96-well

conical-bottom plate. Once cells from each activation timepoint were all harvested, the 96-well plate was centrifuged 4 min 400 g at 4°C, and cells were resuspended in 100μL fixation and permeabilization buffer before being intracellularly stained for IRF4 and RelA on the next day, as explained above. At the end of the staining, cells were resuspended in 50μL PBS with 1 μg/mL Hoechst 33342 (ThermoFisher, #62249), transferred to 1.5mL eppendorf tubes, and shipped at 4°C to the Flow Cytometry Facility of the University Lausanne (UNIL).

Samples were acquired on a 2 camera, 12 channel ImageStreamX imaging flow cytometer (Cytek Biosciences) at low speed and highest magnification (60×). Cells were excited using a 405 nm laser (40mW), a 561 nm laser (200mW), a 642 nm laser (150mW) and a 785nm Side Scatter (SSC) laser (1.5 mW). Only events with a bright field area greater than 1 μm^2 (to exclude cell debris) and non-saturating pixels (Raw max pixel values below 4096) were collected. Data was acquired for at least 10,000 events/sample. Experimental samples contained images for brightfield (Channels 1 and 9), RFP (Channel 3), IRF4-PECy7 (Channel 6), Hoechst 33342 (Channel 7), NF-κB AF647 (Channel 11) and Side Scatter (Channel 12). Data analysis was done using Image Data Exploration and Analysis Software (IDEAS) version 6.3 (Cytek Biosciences). NF-κB nuclear translocation was analyzed using the Nuclear Translocation Wizard in IDEAS software, which creates an analysis template for measuring the nuclear translocation of a probe, in this case NF-κB. This wizard uses the Similarity score which calculates a pixel-by-pixel correlation of the nuclear Hoechst 33342 image to the NF-κB AF647 image. The similarity score quantifies the correlation between two spectrally distinct images of a single cell and is derived from the Pearson's correlation coefficient of the pixel intensities of the image pair.[70,71] It represents how similar the NFκB image is to the Hoechst image in the same cell. Negative similarity scores indicate the images are opposite (NFκB is in cytosol) whereas high similarity scores (≥1) indicate the images are positively correlated (NFκB is translocated to the nucleus). Scores close to zero indicate uncorrelated images.[70,71]

Intracellular staining prior to RNA extraction

When cells were sorted to extract their RNA, the RNase inhibitor RNasin Plus (Promega, #N2615) was used once the cells had been permeabilized. Precisely, following labeling with the eFluor780 viability probe and anti-CD8β antibody, cells were washed 2× with PBS EDTA 1mM HS 1% and then resuspended in PBS, as previously explained. From there, cells were transferred to a new sterile RNase-free 96-well conical-bottom plate, and all further manipulations were carried out under RNase-free conditions. Fixation/permeabilization for 12h–16 h at 4°C was carried out in the presence of 2U/μL RNAsin Plus, washes were done in presence of 0.04U/μL RNAsin Plus, intracellular labeling in presence of 2U/μL RNAsin Plus. During FACS ARIA III sorting (BD Biosciences), cells were kept in permeabilization buffer with 0.4U/μL RNAsin Plus, and cells were collected in 1.5mL eppendorf tubes in permeabilization buffer with 0.04U/μL RNAsin Plus. RNAse-free water (Ambion, #AM9906) was used to prepare permeabilizations buffer.

RNA extraction from fixed and permeabilized cells

Fixed and permeabilized sorted cells collected in 1.5mL eppendorf tubes were centrifuged at 870g for 10 min at 4°C. Cells were resuspended in protease digestion buffer (ThermoFisher, #AM1975) and incubated for 1h at 60°C. Samples were homogenized by vortexing, flash-frozen in liquid nitrogen, and kept at −80°C until RNA extraction. To extract RNA, the RecoverAll Total Nucleic Acid Isolation kit (ThermoFisher, #AM1975) was used according to manufacturer instructions. RNA eluted in 60μL RNAse-free H$_2$O was then precipitated with 6μL of sodium acetate 3M (ThermoFisher, #AM9740), 20ng glycogen (ThermoFisher, #R0551), and 200μL of glacial ethanol 100% (VWR, #20821.310). Samples were incubated overnight at −20°C and then centrifuged at 14,000g for 30 min at 4°C. Samples were washed twice with glacial ethanol 75% and centrifuged at 14,000g for 10 min at 4°C. After removal of the supernatant, samples were dried at room temperature and then resuspended in 4.5μL RNAse-free water (ThermoFisher, #AM9906).

RNAseq libraries construction, sequencing, and analysis

Libraries were homemade using the SMART-Seq2 protocol.[72] Briefly, 1.5μL RNA isolated from fixed and permeabilized cells was retrotranscribed for 90 min at 42°C followed by 10 cycles of 2 min at 50°C and 2 min at 42°C in the presence of 10U/μL SuperScript II reverse transcriptase (ThermoFisher, #18064071), 1μM of 5′ biotin-TEG oligo-dT (AAG-CAG-TGG-TAT-CAA-CGC-AGA-GTA-CTT-TTT-TTT-TTT-TTT-TTT-TTT-TTT-TTT-TTT-TVN) and 1μM of 5′ biotin-C6 template switch oligo (TSO) (AAG-CAG-TGG-TAT-CAA-CGC-AGA-GTA-CAT-997 with 9 = RNA G and 7 = LNA G) (Eurogentec). The resulting cDNA was amplified over 14 cycles of 20 s at 98°C, 15 s at 67°C and 6 min at 72°C, in the presence of 0.02U/μL KAPA HiFi HotStart DNA polymerase (Roche, #07958897001) and 100nM of 5′ Biotin-TEG oligo IS PCR (AAG-CAG-TGG-CAA-CGC-AGA-GT) (Eurogentec). Amplified cDNA was purified with 0.9 volume of AMPure XP paramagnetic beads (Analis, #A63881) for 1 volume of sample, then assayed with the QuantiFluor dsDNA System kit (Promega, #E2670). DNA was tagged for 5 min at 55°C in the presence of Tn5 transposase and the primers supplied with the tagging kit (Illumina, #FC-131-1096). The tagged DNA was then amplified over 11 cycles of 10 s at 95°C, 30 s at 55°C, and 30 s at 72°C in the presence of the indexed primers supplied with the kit (Illumina, #FC-131-2004). The amplified and indexed product was purified with 0.8 volume of AMPure XP paramagnetic beads per 1 volume of sample, then assayed with the QuantiFluor dsDNA System kit. Concentrations were normalized and an equal quantity of each sample was pooled to obtain an equimolar library of up to 16 samples pooled together. The resulting library size was verified by capillary electrophoresis on the TapeStation (Agilent, #5067–5588, #5067–5589). The libraries were sequenced by Genewiz on the Illumina HiSeq platform.

Approximately 380.10^6 pairs of 150bp reads per sequencing line were obtained, which means around 20–25 million pairs of 150bp reads per sample.

RNAseq data analysis and GSEA

After a quality check of the FASTQ files, adaptor sequences were removed, and nucleotides of low read quality removed from the reads using Trimmomatic. File quality was checked again. Trimmed reads were aligned to the GRCh38 human reference genome with HISAT2. Reads count was determined with featuresCount, and normalization of reads count and analysis of differentially expressed genes were performed using DESeq2. Data were visualized with Qlucore Omics Explorer (Qlucore, Lund, Sweden). Gene set enrichment analyses (GSEA) were performed with Qlucore Omics Explorer on 51 gene set. We ran a first GSEA analysis on the "hallmark" gene collection (50 gene sets),[73] version h.all.v2023.2, from the MSigDB database (UC San Diego, Broad Institute), along with the NF-κB target gene signature curated and maintained by the Gilmore Lab at Boston University. From the latter signature, we removed genes that have not clearly been shown to be controlled by NF-κB, as indicated (https://www.bu.edu/nf-kb/gene-resources/target-genes). We ran another independent GSEA analysis on an "exhaustion" gene collection that we compiled from published works.[11,17–20,36,74] GSEA settings were as follows: gene ranking was done by paired t test and the significance of the enrichment score calculated using the gene permutation method (1000 iterations done) rather than the phenotype permutation method, given our limited number of samples. We consequently used a more stringent FDR cutoff ($q < 0.01$). The results of the hallmark gene collection and the exhaustion gene collection can be found in supplemental information as Table S1. List of leading-edges genes that contributed to enrichment score of the GSEA showed in Figure 5 are available in supplemental information as Table S2. The RNAseq data are available at Gene Expression Omnibus database under accession number GSE245739.

Preparation of RNA for RT-qPCR of *IFNG, TNFA, CSF2 and PDCD1*

Human CD8 T cells were subjected to CRISPR/Cas9 (optimized protocol described in dedicated section) and 40,000 cells were activated in round-bottom 96-well plate for 2 days with 13,333 anti-CD3/CD28 beads in 200 μL complete medium supplemented with 500IU/mL IL-2. Frozen human CD8 T cells at day 2 post doxycycline induction were thawed overnight at 37°C 8% CO_2 with 500IU/mL IL-2, 1 μg/mL doxycycline, 5Kunitz/mL DNAse I, and 40,000 cells were activated in anti-CD3 (OKT3 1 μg/mL) coated wells of a round-bottom 96-well plate for 2 days. Cells were labeled at 4°C with viability dye, anti-CD8β and anti-PD-1 antibodies for 20 min. After 2 washes, cells were resuspended in PBS EDTA 1mM HS 1% and FACS-sorted with the Sony MA900 sorter (Sony Biotechnology). Cells were sorted through 100 μm chips in semi-purity mode, and collected in 1.5mL eppendorfs tubes containing 700 μL PBS. Temperature was maintained at 4°C throughout the whole sorting procedure. We usually collected between 15,000 and 30,000 cells.

For cytokine genes expression measurement, 40,000 nucleofected cells were activated in round-bottom 96-well plate for 5 days with 13,333 anti-CD3/CD28 beads in 200 μL complete medium supplemented with 500IU/mL IL-2. Cells were counted and reactivated or not for 4h in high-binding 96-well flat-bottom plates coated or not the night before with 100 μL PBS containing 1 μg/mL anti-CD3 (OKT3 1 μg/mL). The same procedure was used for lentivirally-transduced CD8 T cells, except that these were activated for 4h at 37°C the day after overnight resting from thawing. At the end of activation, cells were labeled at 4°C, washed, resuspended in PBS EDTA 1mM HS 1% and FACS-sorted with the Sony MA900 sorter (Sony Biotechnology), as explained. We usually collected around 25,000 cells. In parallel, cytokine production was measured at the protein level (see dedicated section).

Sorted cells in PBS were centrifuged at 880g for 5 min RT°C, and resuspended in 100 μL of Extraction Buffer from the PicoPure RNA isolation kit (ThermoFisher, #KIT0204). RNA extraction was performed following manufacturer instructions. RNA was eluted in 11 μL RNAse-free water and frozen at −80°C.

RT-qPCR for *IFNG, TNFA, CSF2* and *PDCD1*

From RNA preparations, 8 μL of RNA was incubated for 5 min at 65°C in presence of 14,6 ng/μL of Random Hexamer Primer (ThermoFisher, #SO142) and 36,5 ng/μL of Oligo(dT)$_{18}$ Primer (ThermoFisher, #SO132) in nuclease-free water (ThermoFisher, #R0581). Then was added a mix containing 1× Reaction Buffer for RT (ThermoFisher, #EP0442), 20U/μL RevertAid Reverse Transcriptase (ThermoFisher, #EP0442), 1 μM of dNTP Mix (ThermoFisher, #R1121) and 1U/μL RNAsin Plus Ribonuclease Inhibitor (Promega, #N261B). Addition of this mix led to a 10 ng/μL final concentration of random hexamer primer and 25 ng/μL final concentration of Oligo(dT)$_{18}$ primer. From there, retro transcription was initiated and run for 90 min at 42°C. The resulting cDNA was diluted 2:3 with Ambion Nuclease-Free water DEPC Treated (ThermoFisher: #AM9906). From the diluted cDNA, 1 μL was mixed in 96-well plate in the presence of 0.3 μM forward primer and 0.3 μM reverse primer (Table S3), 0.16 μM of Probe 5′ 6-FAM 3′ TAMRA, 1× Takyon ROX Probe and 1× MasterMix dTTP blue (Eurogentec: #UF-RPMT-B0701) in Ambion Nuclease-Free Water DEPC Treated (ThermoFisher: #AM9906). The qPCR program was 2 min at 95°C followed by 40 cycles of 10 s at 95°C and 1 min at 60°C and was run on a Quantstudio 3 Real-Time PCR System (Applied Biosystems). The data obtained by the Quantstudio 3 Real-Time PCR System were then processed in excel. Technical triplicates were made for each gene expression measurement, and the averaged value was used. If one Ct value in a triplicate deviated from the averaged Ct value with more than 0,5 Ct, this value was discarded. The averaged Ct value for *IFNG*, *TNFA*, *GCSF2* and *PDCD1* was then normalized to each

reference gene (*SDHA, EEF1A1, RPS18*). The $2^{-\Delta\Delta CT}$ value was then used to calculate fold-change between experimental and control condition. Unstimulated T-cells samples were always used to control for the upregulation of *IFNG*, *TNFA*, *GCSF2* and *PDCD1* upon TCR activation.

QUANTIFICATION AND STATISTICAL ANALYSIS

Statistical analyses were performed with GraphPad Prism (GraphPad, San Diego, California), except for RNA-seq data for which paired samples analysis was done with DESeq2 and GSEA performed in Qlucore Omics Explorer. Statistical tests used are indicated in the figure legends.